Yadav *et al. Biotechnology for Sustainable Materials* (2026) 3:8
https://doi.org/10.1186/s44316-026-00058-1

Biotechnology for Sustainable Materials

RESEARCH Open Access

A green approach for remediation of hexavalent chromium [Cr (VI)] from tannery effluent using rice hull biochar and assessing its impact on germination of *Cicer arietinum* (Chickpea)

Smriti Yadav[1], Nikita Kundu[1], Ananya Bhattacharya[1], Palak Khinvasara[2], G. K. Aseri[1*] and Neelam Jain[3*]

Abstract

The leather industry in India contributes significantly to water pollution through the discharge of hexavalent chromium [Cr (VI)]. Conventional Cr (VI) removal techniques are costly and environmentally unsustainable. This study presents an eco-friendly approach of Cr (VI) remediation from tannery wastewater using rice hull biochar (RHB). This study demonstrates the efficacy of RHB as a sustainable biosorbent for hexavalent chromium [Cr(VI)] removal from tannery effluent. Under optimized conditions—pH 4, biosorbent dosage of 0.8 g/L, and contact time of 120 min, RHB achieved 91% Cr (VI) removal efficiency with a maximum adsorption capacity of 10.54 mg/g. Characterization studies revealed that RHB has a specific surface area of 81.80 m^2/g, an average pore size of 3.32 nm, and a Type IV isotherm with H4 hysteresis loop, confirming its mixed microporous-mesoporous structure suitable for heavy metal adsorption. FTIR analysis identified key functional groups (hydroxyl, amine, and carbonyl) responsible for chromium binding, while SEM-EDS confirmed the heterogeneous porous morphology. Kinetic analysis demonstrated that the adsorption process follows pseudo-second-order kinetics ($R^2 > 0.98$), indicating chemisorption as the dominant mechanism. Intraparticle diffusion modelling revealed a two-stage adsorption process involving boundary layer diffusion and intraparticle diffusion. Isotherm studies showed excellent fits to both Langmuir ($R^2 = 0.95$) and Freundlich ($R^2 = 0.96$) models, with Freundlich parameters ($K_f = 4.040$, $1/n = 1.133$) suggesting favourable multilayer adsorption. The study evaluated the phytotoxicity of treated effluent through *Cicer arietinum* seed germination trials. Seed germination trials demonstrated that treated effluent at a 1:4 dilution ratio (20% effluent, 80% biochar residue) significantly enhanced root length, shoot length, leaf number, nodule formation, and fresh/dry biomass compared to controls. It confirmed the detoxification of chromium and suitability for agricultural reuse. These findings establish RHB as a cost-effective, eco-friendly biosorbent that transforms

*Correspondence:
G. K. Aseri
gkaseri@jpr.amity.edu
Neelam Jain
njain1@jpr.amity.edu

Full list of author information is available at the end of the article

© The Author(s) 2026. **Open Access** This article is licensed under a Creative Commons Attribution-NonCommercial-NoDerivatives 4.0 International License, which permits any non-commercial use, sharing, distribution and reproduction in any medium or format, as long as you give appropriate credit to the original author(s) and the source, provide a link to the Creative Commons licence, and indicate if you modified the licensed material. You do not have permission under this licence to share adapted material derived from this article or parts of it. The images or other third party material in this article are included in the article's Creative Commons licence, unless indicated otherwise in a credit line to the material. If material is not included in the article's Creative Commons licence and your intended use is not permitted by statutory regulation or exceeds the permitted use, you will need to obtain permission directly from the copyright holder. To view a copy of this licence, visit http://creativecommons.org/licenses/by-nc-nd/4.0/.

agricultural waste into a valuable resource for industrial wastewater treatment, supporting circular economy principles and Sustainable Development Goals through water recycling and agricultural applications.

Keywords *Cicer arietinum* (Chickpea), Hexavalent chromium [Cr(VI)], Rice hull biochar, Seed germination, Sorption, Tannery wastewater

Graphical Abstract

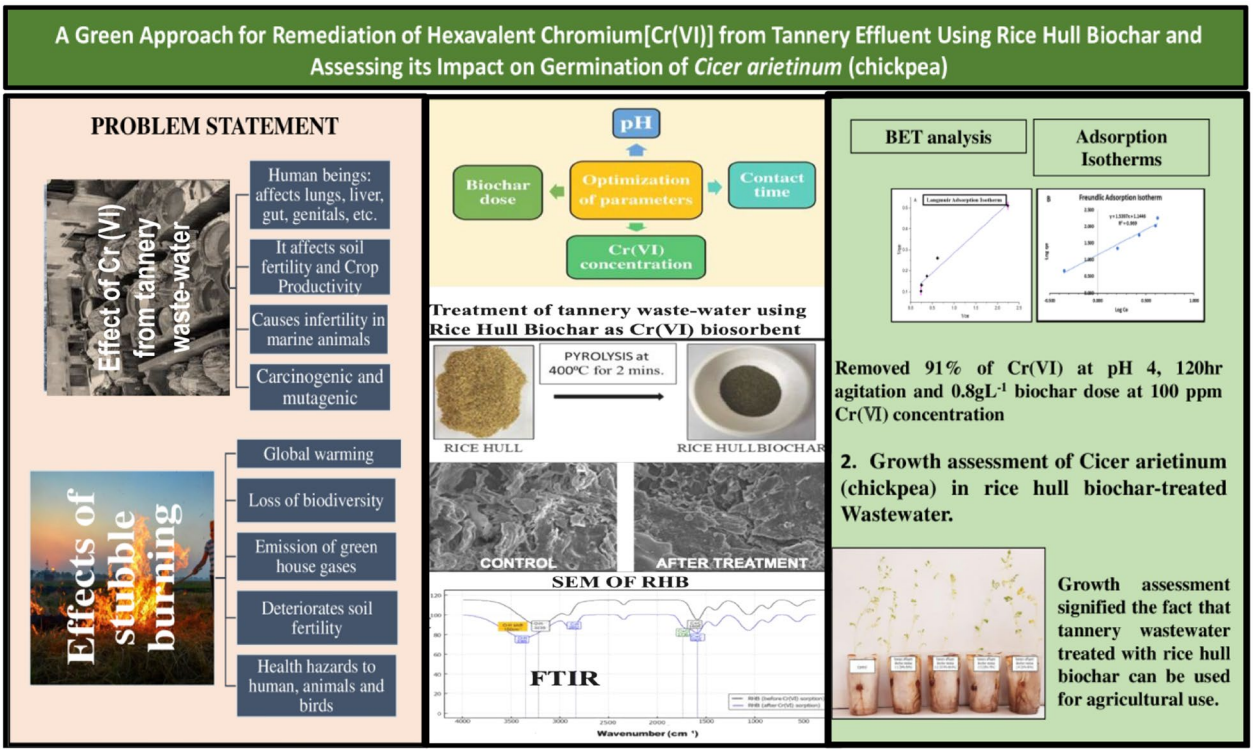

Introduction

Heavy metal pollution has become a significant environmental issue due to rapid population growth and advances in industrialization and urbanization [1]. Over two million tons of wastewater from domestic, industrial, and agricultural sources are released into the global water environment daily [2]. Primary heavy metals of concern include zinc, chromium, lead, cadmium, silver, and copper [3]. Hexavalent chromium [Cr(VI)] is a Class I human carcinogen, with toxic properties that can spread to humans, animals, and plants through the food chain [4]. Exposure to Cr(VI) can cause respiratory and gastrointestinal ailments, skin allergies, and interference with plant and animal growth [5]. Traditional methods, such as precipitation, solvent extraction, reverse osmosis, and ion exchange, are costly and impractical due to high capital expenses and energy requirements [2]. Adsorption has emerged as a cost-effective and efficient technique for removing Cr(VI) from contaminated water [6, 7]. Activated carbon is widely used in wastewater treatment despite the high cost [8, 9]. Research into less expensive and environmentally friendly substitute materials is needed. Agri-residues based biochar can serve as a potent and eco-friendly alternative for bioremediation of heavy metals and large scale industrial waste water treatment. Burning rice waste (rice hull) is a major environmental issue in India, particularly in Punjab, Haryana, and Uttar Pradesh [10]. It is often used to clear fields quickly, but it has detrimental effects on the environment and human health. It releases greenhouse gases such as carbon dioxide, methane, and nitrous oxide [11]. Rice hulls account for 10–20% of the global annual rice production of 500 million metric tons [12]. Various reports have investigated the use of sugarcane bagasse, sawdust, rice husk, aquatic plants, coconut husk, neem bark, and groundnut husk for biochar production and for removing

heavy metals from wastewater [13–15]. The objective of this study was to investigate the use of rice hull biochar (RHB) for removal of Cr (VI) from tannery effluent and determine the effect of treated tannery effluent on seed germination and growth of Cicer arietinum (chickpea) using RHB as an adsorbent.

The novelty of this research lies in its integration of cost-effective chromium remediation, agricultural waste valorization, and safe use of wastewater for agricultural purposes. While previous research has explored various biochar for heavy metal removal, this work uniquely demonstrates that RHB prepared through a simple, energy-efficient pyrolysis process (400 °C for 2 min) achieves 91% Cr (VI) removal efficiency at optimal conditions (pH 4, 0.8 g/L biochar dose, 120 min), comparable to more complex biosorbents while requiring lower doses and shorter processing times. The novelty extends beyond removal efficiency to include comprehensive mechanistic elucidation through combined FTIR, BET, SEM-EDS, and kinetic analyses, revealing a multi-modal chemisorption mechanism involving electrostatic attraction, surface complexation, ion exchange, and potential catalytic reduction facilitated by indigenous metal oxides. Most significantly, this study pioneers the demonstration of post-treatment application by validating that treated tannery effluent, when combined with biochar residue at a 1:4 dilution ratio, not only eliminates phytotoxicity in Cicer arietinum (chickpea) but also actively enhances plant growth parameters (root length, shoot length, nodulation, and biomass) beyond control levels establishing a complete circular economy framework where agricultural waste (rice hull) is converted into a dual-function material that simultaneously remediates industrial wastewater and serves as a growth-promoting soil amendment, thereby addressing Sustainable Development Goals (SDGs) 6, 12, 14 and 15 while providing practical solutions for water-scarce regions requiring safe wastewater reuse in agriculture.

Materials and methods

Biomaterial collection and preparation

Rice hull (RH) biomaterial was collected from local farmers and washed in autoclaved distilled water. It was sun-dried for 2 days and oven-dried at 60 °C for 2–3 days. The RH was then ground and sieved. For the preparation of RHB (Fig. 1), RH was pyrolyzed at 400 °C for 2 min in a muffle furnace, then cooled. After returning to normal temperature, it was converted into powder and stored in an air-tight box [16].

Design of the batch sorption experiment for chromium adsorption

Batch sorption experiments were performed in 50 mL Falcon tubes under constant shaking at 120 rpm at room temperature. A 0.01 M NaCl solution was used as the electrolyte and the working solution. Cr (VI) level (100–500 ppm) was used for the experiment under different conditions, as explained below [17]. The experiments were carried out in triplicate. The diphenylcarbazide (DPC) method was used to estimate chromium concentration [18].

Optimization of different parameters for efficient chromium removal by RHB

Effect of pH

To maintain the pH of the working electrolyte NaCl solution, HCl and NaOH were added.1% (w/v) RHB and 100 ppm Cr were added to 20 mL of NaCl solution. The pH range was set to 2–8 in Falcon tubes, which were kept in a shaking incubator for 120 min. Samples were filtered, and chromium content was estimated.

Chromium concentration

The study involved adding [Cr (VI)] 100–500 ppm concentration values to the electrolyte solution, each with a pH of 4 and 1% (w/v) biochar dose. The samples were shaken for 120 min, filtered, and used for chromium estimation.

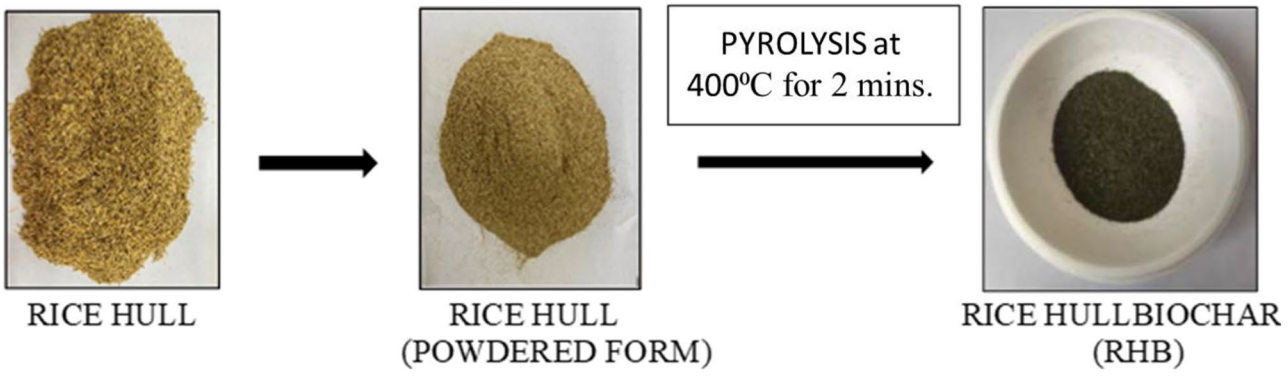

Fig. 1 Preparation of RHB

Biochar dose

Various doses of RHB (0.2, 0.4, 0.8, 1, 1.2 g/L) were added with 100 ppm [Cr (VI)] concentration in all samples at pH 4. Samples were shaken at 120 rpm at room temperature. After centrifugation, samples were filtered. Chromium in the filtrates was estimated.

Contact time

The shaking contact time was changed to 30, 60, 90, and 120 min, approximately, while keeping the chromium concentration at 100 ppm and the biochar dose at 0.8 g/L constant. Centrifugation was done, and samples were filtered for chromium analysis.

Analysis of hexavalent chromium by diphenyl carbazide method (DPC method)

The Diphenylcarbazide method was used to determine the concentration of hexavalent chromium in each sample. At 4 °C, 10 mL of the filtrate was centrifuged at 10,000 rpm for 10 min. The supernatant was used with the UV-VIS double beam spectrophotometer (Systronics 2202TS) to measure Cr(VI) at 540 nm [18].

Mathematical calculation for Chromium [Cr (VI)] removal by RHB

$$\%\ of\ C_r\ removal = \frac{C_0 - C_f}{C_0} \times 100$$

Where,

C_0 (mg/L) = Initial chromium concentration.

C_f (mg/L) = Final chromium concentration.

Surface analysis of RHB by FTIR spectroscopy, SEM, EDS, and BET

By collecting Fourier Transform InfraRed (FTIR) spectra (PerkinElmer Spectrum IR Version 10.6.1) spanning 400–4000 cm^{-1} wave number, the functional groups present on the surface of rice hull were identified. Field-emission scanning electron microscopy (FESEM) and energy dispersive X-ray spectroscopy (EDS) (TESCAN MIRA-LMS) were used to analyse the surface morphology of RHB before and after treatment with chromium Cr (VI). Brunauer–Emmett–Teller (BET) (BELSORP Data Analysis Software BEL Master - Ver 7.2.0.4) is used to analyze the specific surface area and pore size of RHB.

Adsorption isotherms

Adsorption isotherms were used to assess metal adsorption capacity on RHB. The Langmuir model supports ion-exchange mechanisms and monolayer adsorption, while the Freundlich model explains multilayer adsorption on heterogeneous surfaces [19]. The isotherm data for metal ion adsorption by RHB were analyzed using various isotherm models.

Langmuir Isotherm [20]

$$q_e = \frac{q_m\, K_L C_e}{1 + K_L C_e}$$

Here;

q_e (mg/g): - amount of metal ion adsorbed at equilibrium.

q_m (mg/g): - monolayer adsorption capacity.

K_L (L/mg): - Langmuir adsorption constant.

C_e (mg/L): - the equilibrium concentration.

Freundlich Isotherm [21]

$$q_e = K_F C_e^{1/n}$$

Here;

q_e (mg/g): - amount of metal ion adsorbed at equilibrium.

K_F (mg/g) (L/mg): - the Freundlich adsorption constant.

C_e (mg/L): - the equilibrium concentration.

n: - is the nonlinearity factor.

Adsorption kinetics and mechanism

Weber-Morris Intra-particle Diffusion Equation.

The Weber-Morris model was developed based on the theory proposed by Crank (1975) for spherical particle diffusion. The model equation is:

$$qt = k_p \times t^{0.5} + C$$

Where:

Q_t = Quantity adsorbed per unit mass of adsorbent at time t.

K_p = Intra-particle diffusion rate constant.

t = Contact time (minutes).

C = Intercept, proportional to boundary layer thickness.

Cicer arietinum (Chickpea) seed germination studies

The study aimed to investigate the potential of RHB to mitigate chromium-induced toxicity in chickpea seeds (*Cicer arietinum*). Tannery effluent was collected from CETP outlets in Manpura Mancheri village in Amber Tehsil of Jaipur, Rajasthan, and analyzed for chromium. Chickpea seeds were sterilized, washed, and soaked in distilled water for 2–3 h. Cotton wool was soaked with Agri-waste extract and tannery effluent in different dilution factors: 1:1 (50%:50%), 1:2(33.5%:66.5%), 1:3 (25%:75%), 1:4 (20%:80%). Triplicates of each treatment were maintained, and parameters like seed germination, root length, shoot length, number of leaves, nodules, fresh mass, and dry mass were measured [22]. The data was then subjected to statistical analysis. The study aimed to determine the potential of RHB in reducing the toxic effects of chromium on chickpea seeds.

The percentage germination rate was calculated by

$$\%\ of\ germination\ rate = \frac{seed\ germinated\ \times\ 100}{total\ seed}$$

Preparation of biochar residue (Agri-Waste Extract)

The RHB was heated in a water bath at 70 °C for 15 min, filtered, centrifuged, and collected. The content was agitated for 24 h, prepared with different dilution factors, and preserved at 4 °C. All treatments were triplicated, and a control treatment was included. The content was preserved at 4 °C, and a control treatment was also included [23].

Results & discussion

Batch sorption parameters

pH

pH plays a crucial role in the sorption process of metal ions, affecting the degree of ionization, surface charge, and metal ion speciation [24]. Changes in pH can stabilize surface charges on the biosorbent, affecting the removal of chromium. Cr(VI) sorption experiments were conducted over the pH range 2–8, revealing that the capacity of RHB for Cr(VI) removal depends on the solution pH (Fig. S1). Lower pH improves heavy metal biochar-mediated adsorption [25], with the removal percentage increasing from 52% to 64% and reaching a maximum of 80% at pH 4. The pH range of 4, at which RHB reaches its optimum, is consistent with trends seen with Cr (VI) and biosorption, although values can vary considerably depending upon the biosorbent. Biosorption of Cr (VI) at lower pH (2–4) occurs due to the dominance of both $HCrO_4^-$ and $Cr_2O_7^{2-}$ ions of Cr (VI), whereas at higher pH, CrO_4^{2-} ions dominate as reported in a study on non-wood based biochars [26]. By contrast, at lower pH, RHB functional groups protonate to positively charged sites that electrostatically interact with negatively charged Cr (VI) ions.

In comparison with other studies, walnut shell biochar has a maximum removal rate of 96.5% at a pH range of 4–5 [16], very close to the results of the current study. The best pH condition for corn straw biochar (CSB) and cow manure biochar (CMB) is at pH 6.0 with adsorption capacities of 21.24 mg/g and 24.28 mg/g, respectively. The adsorption process was primarily governed by monolayer chemisorption [27]. This variation indicates a differing nature of the surface chemistry of functional groups of RHB from these two. Another interesting result was observed for reduced rice straw biochar with a removal rate of 95% at a very acidic pH 2 [28], which confirmed the crucial role of pyrolysis conditions as well as raw material composition. The variation in the optimal pH can be attributed to differences in the points of zero charge, depending on the type of biochar, ash content, surface functional group chemistry, and levels of carbonization.

The reduction in removal efficiency at greater pH values (>6) has also been consistent in most biochar studies, and this can be attributed to two different processes: (1) deprotonation of the surfaces of biochar, causing it to become negatively charged, thus repelling anionic chromate ions, and (2) competition between hydroxyl ions and adsorption sites. The pH-dependent removal efficiency of chromate ions has practical applications in wastewater treatment, where most industrial effluent streams tend to be slightly acidic to neutral, making RHB an ideal choice in this area, with little need to adjust the pH.

Chromium concentration

The removal rate of chromium is influenced by the concentration of chromium Cr(VI). Various concentrations of Cr(VI), 100 ppm to 500 ppm, were added at pH 4 with a contact time of 120 min, resulting in a maximum removal rate of 85% at 100 ppm. However, as the concentration increased, the removal rate decreased, with only 67% of chromium remediated at 500 ppm (Fig. S2). The inverse proportion between the initial concentration of chromium ions and the removal efficiency is a widely acknowledged fact for biosorption processes. The decrease of 18% from 85% to 67% in removal efficiency as the concentration changed from 100 ppm to 500 ppm for RHB indicates a fixed number of binding sites available for metal ion adsorption. The dependence of this process on concentrations is also well supported by standard principles of adsorption. At lower concentrations, there is a higher proportion of binding sites compared to metal ions available for adsorption. As such, at higher concentrations of metal ions, saturation of available binding sites occurs at a quicker rate. This results in lower percentages of metal ion removal with higher amounts of metal ion being adsorbed [29].

Comparison with earlier findings in the literature shows similar trends but with differences in the sensitivity to concentrations. The results for banana peel biochar were found to have much more pronounced reductions in removal efficiency of around 50% for Cu^{2+} and 70% for Pb^{2+} at higher concentrations [30], implying that RHB has better resistance to deactivation by concentration. These enhanced capabilities can be due to the increased specific surface area of RHB with 81.80 m^2/g, along with good porosity with average pore diameters of 3.32 nm. This might be due to rapidly filled binding sites and saturation of sorption sites on the surface [31]. The concentration effect is also very important in the adsorption mechanism. The small decrease in removal efficiency indicates that there may be more than one adsorption mechanism occurring concurrently. Surface complexation is

prominent in low concentrations, while ion exchange or precipitation may occur in higher concentrations. Experiments done on coffee husk biochar [32] indicated that optimum conditions required for 98.1% removal of Pb (II) were pH 6.0, 0.15 g dosage, and 180 min, and pH 6.9, 0.05 g dosage, and 135 min were required for 96.3% removal of Cu (II) which was much longer than that was attained in our experiment at pH 4.0, 0.8 g for 120 min for RHB, which indicates that adsorption is quicker in case of RHB. Moreover, concentration-dependent data helps to understand the applicability prospect. For industrial effluents containing differing concentrations of chromium, it can be perceived from the results that RHB will prove most economical for the treatment of moderately to low concentration wastewaters containing 100–300 ppm chromium at efficiencies above 75%, and for wastewater containing higher concentrations, a two-stage treatment process may be required [28].

Biochar dose

The study examines the impact of RHB dose on chromium removal. The biosorbent dose effect was tested with 100 ppm Cr(VI), a pH of 4, and a 120-minute contact time. Results showed that increasing the RHB dose increased the removal rate of Cr(VI). As the dose increased from 0.2 g/L to 0.8 g/L, 90% of Cr(VI) was removed (Fig. S3), since an increase in RHB dose provides more exchangeable sites for chromium ions, as well as more functional groups, which result in stronger metal cation-biochar interactions [28, 33]. However, the Cr(VI) remediation percentage decreased from 90% to 84% as the biochar dose increased from 0.8 g/L to 1.2 g/L. The S-curve patterns of the biphasic response of the biosorbent dose in this experiment, first increasing and then plateauing and slightly decreasing, are typical of heterogeneous adsorption systems. The dose of 0.8 g/L for 90% removal efficiency, as indicated by this S-curve pattern, approximates functionality in terms of site efficiency and mass transfer rates. There are various explanations regarding this phenomenon that have been dealt with in other comparative biochar studies [34].

The rise in removal efficiency values from 0.2 g/L to 0.8 g/L can be primarily attributed to the proportional increase in the total number of active adsorption sites. At every stage, with an increase in the biosorbent concentration, a rise in functional groups such as hydroxyl, carboxyl, and amine is also observed. The decline at a modest rate of 6% with a rise in concentration from 0.8 g/L is an interesting aspect of the result that does not align with other literature sources, where efficiency is often seen plateauing and not falling [25]. There could be several reasons for this reduction, like the aggregation and agglomeration of particles at higher biosorbent concentrations, higher viscosity of the solution, and lower rates of mass transfer, screening effects where the external particles protect the inner particles from accessing the adsorbable species, and incomplete mixing and sedimentation due to the higher density of the suspension. Similar results have been observed for pistachio shell powder and fruit cortex waste for the removal of heavy metals [33, 35], although the optimal capacities varied (typically 1–2 g/L), indicating that RHB could provide better performance at lower capacities, thus being more cost-effective.

The dose-dependent study is also an important source of information regarding adsorption capacity and economy. With an optimal dose of 0.8 g/L for removing 90% of 100 parts per million of Cr (VI) ions, the adsorption capacity per unit mass is calculated to be nearly 11.25 mg/g, which is in very good agreement with the obtained result of 10.54 mg/g for q_{max} from isotherm analysis. In comparison to various types of biochar, the concentration of 2.0 g/L of coffee husk biochar was required to remove heavy metals at a concentration of 5.0 mg/L [36]. Higher efficiency of RHB in utilizing the dose can be attributed to its optimum pore size distribution of 3.32 nm and its Type IV isotherm with an H4 hysteresis loop, which reveals that its mesopores are of slit-shaped morphology and can be accessed easily compared to other biochars. In practical application terms, it is economically important to determine 0.8 g/L to be a concentration at which the maximum dose is achieved [37]. In overdosing, not only is there an unnecessary consumption of biosorbent material, but there may also be complications in post-process solid-liquid separation. It is important to note that there is a slight drop-off in effectiveness past the point of optimum dosages.

Contact time

The study reveals that RHB performs better in Cr(VI) ions removal due to its agitation time. The adsorption of chromium surges with increasing agitation time, with a reduction of 83% of chromium Cr(VI) ions remediation at 30 min and 91% at 120 min. The sorption kinetics have two phases: a rapid phase and a slower phase. The biphasic kinetics evidenced by RHB, with a rapid initial adsorption (83% in 30 min) accompanied by a slower approach to equilibrium (91% at 120 min), is typical of processes largely controlled by chemisorption and reveals very important information on rate-limiting steps and mechanisms (Fig. S4) [37]. This kinetics are consistent with pseudo-second-order kinetics ($R^2 > 0.98$) discussed in Sect. "Adsorption kinetics and mechanism", supporting the notion of a mechanism largely dominated by chemical forces rather than physical adsorption.

It can be assumed that this initial rapid stage is due to the existence of many free binding sites along with a high concentration gradient in the initial stage of reaction.

During this stage, external mass transfer control (boundary layer diffusion) is observed, allowing chromate ions easy access to adsorption at surface functional groups. After that, a slow stage, reflecting a shift in control from external to intraparticle diffusion, where chromate ions diffuse inside the pore structure of the biochar particles into inner adsorption sites, occurs. This two-step process of intraparticle diffusion was validated in Sect. "Adsorption kinetics and mechanism". Such a comparison using literature indicates that there is a considerable difference in the time taken for equilibration among various biochar and experimental setups. For example, 180 min were required for equilibrium to be attained for coffee husk biochar at a heavy metal concentration of 5.0 mg/L [36], which is 50% higher than RHB, although the latter operates at a lower heavy metal concentration. It can be noted that RHB has a preferable mass transfer property, which can be attributed to its developed mesoporous structure (Pore size of 3.32 nm). Meanwhile, a Type IV with H4 loop of the isotherm, as also confirmed by BET, specifies slit-shaped pores with a preferable diffusion property because of the narrower width of the slit-shaped pores.

The 8% removal ability from 30 to 120 min, though appearing small, corresponds to about 10% of the total adsorption capacity, which is important for attaining high removal efficiencies. The above-mentioned scenario might be attributed to the hierarchical pore structure of RHB, where the mesopores work as highways for rapid adsorption, followed by the micropores in the slow adsorption stage. The kinetic profile also gives useful hints for industrial-scale applications. The result that 91% of total removal is attained after a period of 30 min may imply that continuous flow systems requiring a contact time of 30–60 min can yield a satisfactory removal process whilst retaining a higher flow rate than batch systems operating at equilibrium conditions. However, to get maximum benefit, a contact time of 120 min would prove useful for batch process removals.

Even so, the fact that walnut shell biochar was able to remove 96.5% of the contaminant [16] as compared to groundnut shell biochar with complete removal of Chromium (VI) in 10 h [38], seems to ensure that there is comparable removal time using groundnut husk biochar. Therefore, it seems that agricultural waste biochars remove contaminants at comparable rates.

FTIR, SEM ‖ EDS and BET analysis

FTIR

The quantitative assessment of functional groups on the RHB surface was performed using FTIR spectra for both RHB without and with chromium Cr (VI). The Fig. 2 illustrates the FTIR spectra of RHB in the absence and presence of Cr (VI). The peak in upper curve at 3235 cm^{-1} represents the H-bond, -OH stretch, while in lower curve the peak shifts to 3385 cm^{-1}, indicating the involvement of macromolecules like pectin, cellulose, and lignin. The bands ranging from 3650 to 3250 cm^{-1} signify the H-bond, confirming the presence of H_2O, hydroxyl (-OH), ammonia, or amino groups [39]. The Chromium (VI) sorption at peak 2852 cm^{-1} depicts the methyl group stretch, and the peak at 2922 cm^{-1} indicates an adsorption band for long-chain linear aliphatic compounds, primarily methylene. In Fig. 2, before Cr (VI) sorption, the peak is at 2361 cm^{-1}, and after Cr VI sorption, it depicts

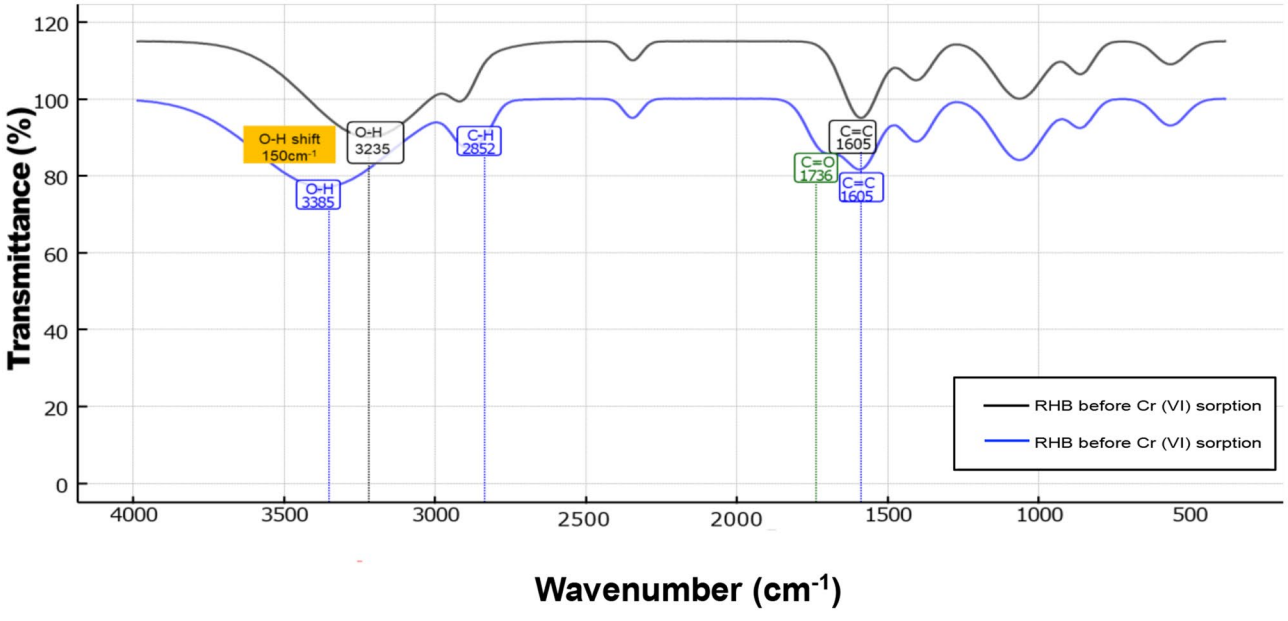

Fig. 2 FTIR spectra of RHB before and after chromium Cr(VI) sorption

the shifts to 2362 cm^{-1} due to the C ≡ C absorption band. The FTIR spectra of RHB after chromium treatment (Fig. 2) reveal peaks at 1736 cm^{-1}, characteristic of simple carbonyl compounds such as aldehydes, ketones, esters, or carboxyl groups. The FTIR spectra of RHB display a strong intensity peak at 1605 cm^{-1}, indicative of a double bond or aromatic compounds. In spent mushroom compost biochar, a strong hydroxyl band at 3400 cm^{-1} was observed, corresponding to the intense adsorption of heavy metals [20, 39]. These bands correspond to the stretching and bending vibrations that facilitate heavy metal removal. Similar results for Cr (VI) sorption were previously noted using almond and apricot shells [33]. The stretching of bands corresponding to hydroxyl (-OH), C-H, and C = O groups in the groundnut shell FT-IR spectra for zinc removal suggests a chemical interaction between zinc ions and functional groups on the adsorbent [22; 32]. The large absorption peak at 3352.05 cm^{-1} in the native sunflower stem indicates a bonded hydroxyl group, while loading with Cr (VI) shifts the OH absorption peak to 3382.91 cm^{-1} [39]. This implies that complexation with functional groups, ionic exchange, and chemical reactions with surface sites may contribute to adsorption on adsorbents.

The spectral shifts that have been noted for pristine and chromium-amended RHB are of very valuable mechanistic significance when one compares these results with those for other biochar systems. The importance of the spectral shift of the hydroxyl stretch peak, for instance, from 3235 cm^{-1} to 3385 cm^{-1} upon chromium sorption can be noted, where there has been a 150 cm^{-1} spectral shift that can be contrasted with a spectral shift of 31 cm^{-1} for sunflower stem biochar that changed from 3352 to 3383 cm^{-1} [40].

The appearance of the carbonyl peak at 1736 cm^{-1} following chromium treatment can be noted and could be an indication of partial oxidation of the surface groups during the adsorption process or the formation of chromium-carbonyl complexes. This finding appears consistent with other results for almond and apricot shell biochar [40], where similar peaks for carbonyl groups appeared following the adsorption processes. The observed presence of both C = O and C-O bands associated with stretching vibrations could indicate chromium binding to carbon through more than one functional group at the same time; this appears consistent with the chemisorption process supported by kinetic modeling. Compared to the Spent Mushroom compost biochar, where the hydroxyl peaks were dominant around 3400 cm^{-1}, which favors the adsorption of heavy metals [41], the peaks of the RHB appear in positions that are similar but different depending upon the hydrogen bonding condition and the type of hydroxyl groups. The methylene bands found around 2922 and 2852 cm^{-1} in the Chromium-loaded RHB indicate that the aliphatic carbon chains of the biochar are unaltered; thus, depicting the structure of the biosorbent remains intact, which is a crucial consideration for its future use as heavy metal biosorbent in agriculture for maintaining soil fertility as observed in a study on rice, maize, wheat, barley husk biochar also [42].

The difference in the range of the absorption peak of C ≡ C (from 2361 to 2362 cm^{-1}) is not much, but it still shows the occurrence of some level of π-electron delocalization in the carbon system after metal complexation. The existence of an intense aromatic band at 1605 cm^{-1} in pristine RHB leads to consideration of π-π stacking, making it an additive component in chromium adsorption, particularly in organometallic chromium compounds possibly existing in biochar. Doing a cross-comparison with groundnut shell biochar for the removal of chromium [38], the similarities in the involvement of the functional groups (hydroxyl, C-H, and C = O) indicate that the adsorption mechanisms of heavy metals are similar for each type of agricultural waste biochar, with varying dominance based primarily on the conditions of pyrolysis. From the FTIR data, a multiple adsorption process can be ascertained that includes electrostatic attraction, surface complexation, ion exchange, and possibly chemical reduction of Cr (VI) to Cr (III) based on the prominent role of the hydroxyl and carbonyl functional groups.

SEM and EDS

The study examined the surface structure and porosity of RHB using SEM analysis [27]. It was observed that biochar's surface was rough, irregular, and uneven, with numerous macro and micro pores (Fig. 3A, B, C and D). This provided ample adsorption sites. The physicochemical interactions between heavy metal ions and functional groups on the biochar's surface are believed to explain this behavior [43]. The EDS graph confirmed the presence of elements like carbon, oxygen, iron, calcium, aluminum, and potassium, which are the main components of biochar and help in the adsorption of heavy metals (Fig. 4).

The SEM morphological analysis of RHB shows the surface features that are important for understanding the adsorption capacity of RHB and provide important information when compared with other biochar samples. The rough, irregular, and heterogeneous surface topography of fresh RHB (Fig. 3A and B) is characteristic of lignocellulosic biochar, which is produced by the pyrolysis process, where the thermal decomposition of organic materials produces a highly porous carbon material [44]. The surface topography of RHB is dramatically different from the smooth surface of other materials and is an important feature for the high surface area and

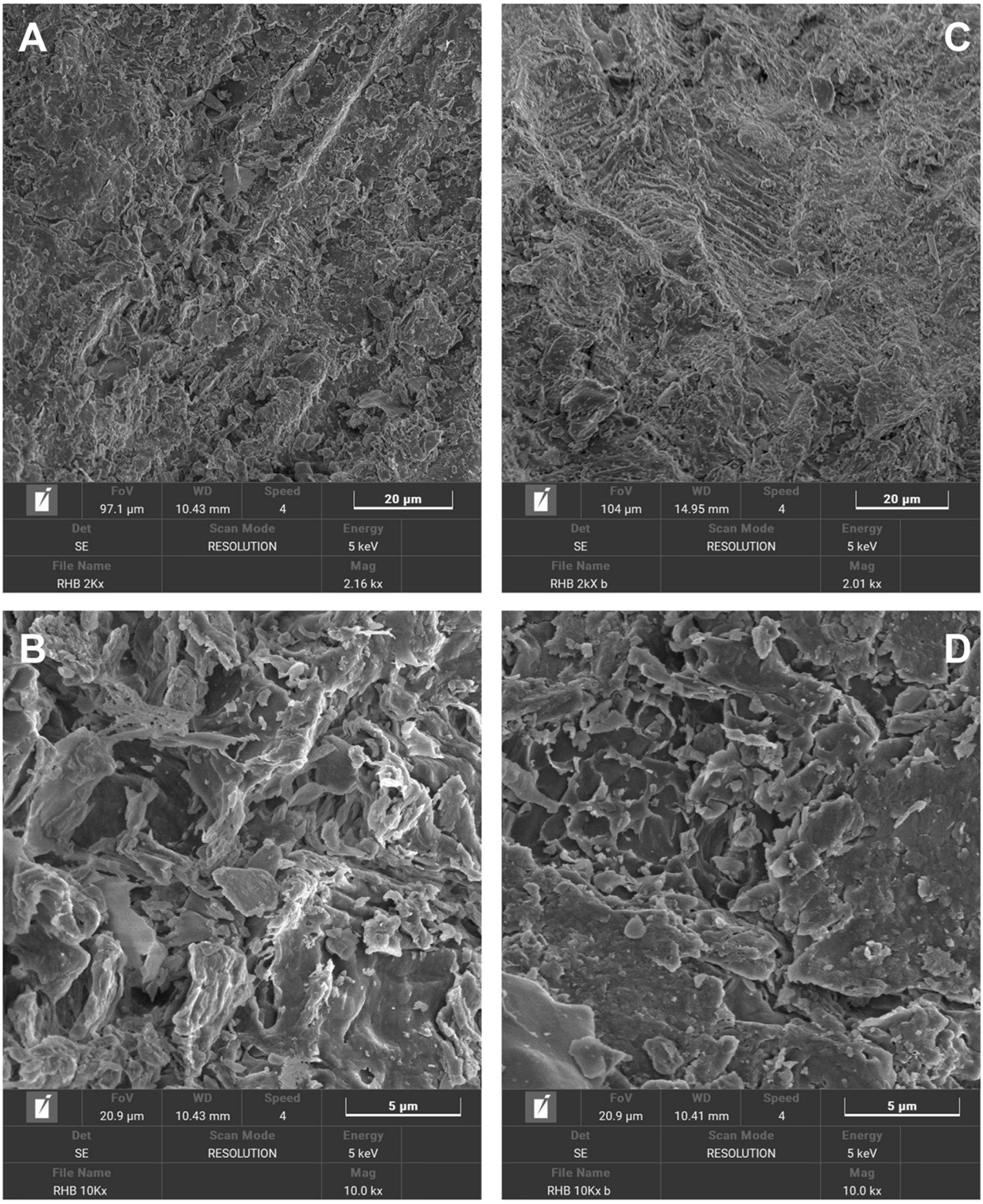

Fig. 3 SEM images of RHB: **A**) Control at 2000X, **B**) Control at 10000X; **C**) Treated RHB at 2000X, **D**) Treated RHB at 10000X

accessibility that are important for efficient metal ion sorption.

The presence of macropores (> 50 nm) and micropores (< 2 nm) as revealed by the SEM images confirms the BET analysis results, which suggest the Type IV isotherm with a combination of porosity [41]. Macropores serve as pathways that facilitate the easy diffusion of chromate ions into the biochar, while micropores are

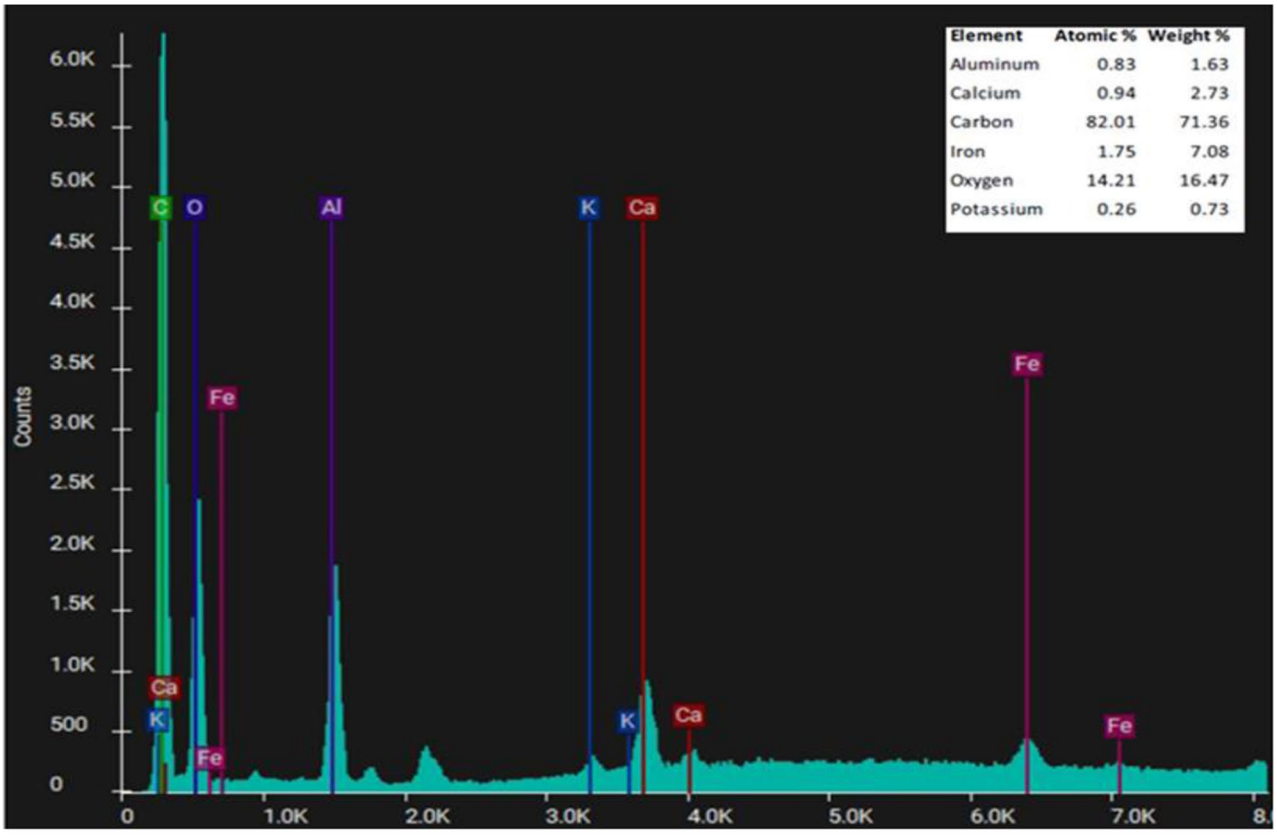

Fig. 4 EDS analysis of RHB

responsible for the highest surface area that is available for the adsorption process to occur. The hierarchical pore structure is more advantageous than the uniform pore structure because it overcomes the diffusion limitation and allows for the maximum utilization of the adsorption capacity. The same hierarchical pore structure has been reported in corn straw biochar and spent mushroom compost biochar [41], but the pore size distribution and surface roughness vary according to the raw material and pyrolysis conditions.

By comparing the SEM images of the before and after chromium adsorption on RHB (Fig. 3A, B, C and D), it is possible to confirm the adsorption. Although the overall porous structure is maintained after chromium adsorption, thus ensuring the structural integrity of RHB during the adsorption process, there could be a slight smoothening of the edges of the pores or the smaller pores being filled. This is important for the regeneration of the biosorbent for reuse, as otherwise, the extent of structural degradation would affect the adsorption process. The structural integrity of the biosorbents is maintained after adsorption, as reported in the studies on walnut shell biochar [16] and groundnut husk biochar [39], although the extent of pore blocking depends on the metal loading and adsorption processes.

The EDS elemental analysis (Fig. 4) provides complementary information that is essential for understanding the adsorption mechanism. The confirmed presence of carbon (the primary structural element) and oxygen (associated with functional groups) is expected for biochar, but the detection of iron, calcium, aluminium, and potassium is particularly significant. These metallic elements, derived from the rice hull's mineral content and concentrated during pyrolysis as the volatile organic components are removed, play multiple roles in chromium adsorption:

1. Ion exchange sites: Calcium and potassium can undergo exchange with chromium species, providing an additional adsorption pathway beyond surface complexation. This mechanism is particularly important at higher pH values, where surface functional groups may be deprotonated [42, 45].
2. Surface charge modification: The presence of metal oxides (likely present as CaO, K_2O, Fe_2O_3, Al_2O_3) influences the point of zero charge (PZC) of the biochar, affecting the pH-dependent adsorption behavior observed in Sect. "pH". These oxides can create positively charged surface sites even at

moderately acidic pH, enhancing the electrostatic attraction of anionic chromate species [46, 47].

3. Catalytic reduction: Iron can facilitate the reduction of Cr (VI) to the less toxic and less mobile Cr (III). This redox-coupled adsorption mechanism, suggested by some researchers [48, 49], would represent an additional removal pathway and could explain the high removal efficiency achieved by RHB.

Comparative EDS analyses of different biochar reveal significant compositional variations. Rice hull biochar typically contains higher silica content (not explicitly mentioned but common in rice-based materials) compared to wood-based biochar like walnut shell [16], which may contribute to different surface chemistry and adsorption behaviour. Spent mushroom compost biochar [41] often shows higher nitrogen content, potentially providing additional functional groups for metal binding. The specific elemental composition of RHB, with its balance of carbon, oxygen, and metal oxides, appears optimized for chromium adsorption, as evidenced by the 91% removal efficiency achieved.

The rough surface morphology combined with the presence of catalytic metals explains why RHB achieves such rapid adsorption kinetics (83% removal in 30 min). The irregular surface creates turbulence at the biochar-solution interface, reducing boundary layer thickness and enhancing mass transfer [49]. Additionally, the exposed metal oxide particles on the biochar surface provide readily accessible high-energy binding sites for initial rapid adsorption, before slower intraparticle diffusion begins to dominate.

Cross-comparison with other agricultural waste biochar shows that surface morphology varies significantly with feedstock type and pyrolysis temperature. Materials pyrolyzed at higher temperatures (> 500 °C) typically show more developed pore structures but may lose some oxygen-containing functional groups, while lower-temperature biochar (300–450 °C, including RHB at 400 °C) retain more functional groups but may have less developed porosity [50]. RHB appears to strike an effective balance, as evidenced by both SEM (showing well-developed porosity) and FTIR (showing abundant functional groups).

One consideration for practical application is the potential for pore blocking with extended use or at very high chromium concentrations. The SEM images of chromium-loaded RHB ideally show minimal pore occlusion, confirming that the biochar can maintain performance over multiple adsorption cycles. The combination of SEM and EDS data thus provides a comprehensive picture: RHB possesses an optimal surface morphology (rough, hierarchically porous) and elemental composition (carbon framework with catalytically active metal oxides and ion-exchangeable cations) that together explain its excellent chromium adsorption performance. These structural and compositional features align well with the functional group analysis from FTIR, the surface area data from BET, and the mechanistic insights from kinetic and isotherm studies, creating a coherent understanding of why RHB performs as an effective biosorbent for hexavalent chromium removal.

BET

Figure S5 represent the N_2 adsorption-desorption isotherms, while Figure S6 shows the pore size distribution of biochar. RHB sample exhibits Type IV isotherm with H4 hysteresis loop, which confirms that the biochar contains slit-like pores, common in carbonaceous materials like biochar [50]. It has a mixed porosity structure (both micropores and mesopores). This result aligns with the pore size distribution analysis and is suitable for adsorption applications (e.g., water treatment, gas adsorption). RHB depicts a Specific surface area (m^2/g) of 81.80, Pore volume (cm^3/g) of 0.12, and average pore size (nm) of 3.32. The BET results show that RHB has good adsorption properties, making it an efficient material for heavy metal (chromium) separation from tannery wastewater. Similar results were obtained from corn stalk biochar for cadmium removal, with a specific surface area (m^2/g) of 92.86 and an average pore size (nm) of 3.15 [51].

The BET characterization results for RHB show that it has a well-developed porous structure with properties that make it better than other biochar materials for adsorbing heavy metals. The specific surface area of 81.80 m^2/g is not as high as that of commercial activated carbon (which is usually between 500 and 1500 m^2/g), but it is still competitive with other biochar made from agricultural waste [53, 56]. It is also a great balance between adsorption capacity and production cost. Even though RHB was made using a simpler and shorter pyrolysis process (400 °C for 2 min) [52]. This suggests that rice hull can be turned into an adsorbent material very efficiently.

Unrestricted access to interior pore surfaces is ensured by the average pore size of 3.32 nm, which is within the mesopore range (2–50 nm) and larger than the hydrated ionic radius of chromate species ($HCrO_4^-$ ~0.4 nm, $Cr_2O_7^{2-}$ ~0.6 nm). This pore size is strikingly like corn stalk biochar (3.15 nm) [51], indicating that agricultural residues derived from rice may have intrinsic structural traits that, when pyrolyzed, produce comparable mesoporous structures.

The Type IV isotherm with H4 hysteresis loop indicates the presence of slit-shaped pores in carbonized plant materials, which enhance surface area and adsorption efficiency. This morphology benefits chromate adsorption due to the alignment of chromate ions with the pore walls, thereby maximizing the interaction strength [51].

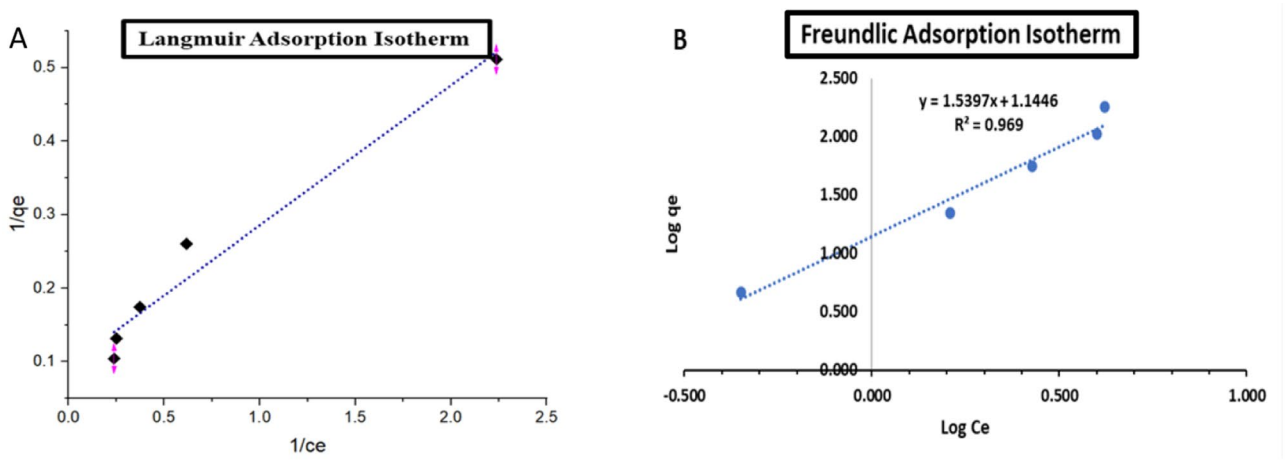

Fig. 5 Adsorption isotherm for chromium metal using (**A**) Langmuir, (**B**) Freundlich isotherm for RHB

Table 1 Langmuir and the Freundlich isotherm characteristics of RHB for Chromium [Cr (VI)] adsorption

Biochar	Freundlich		Langmuir			
Rice hull Biochar	K_F	1/n	R^2	q_{max} (mg/g)	K_L	R^2
	13.95	1.53	0.96	10.54	0.49	0.95

The mixed microporous-mesoporous structure supports biphasic adsorption kinetics-mesopores facilitate rapid initial diffusion, while micropores allow for slower secondary adsorption phases. The biochar's pore volume of 0.12 cm^3/g represents 14.6% porosity, balancing sufficient adsorption capacity with mechanical integrity. Compared to other biomass-derived adsorbents, RHB exhibits competitive BET characteristics, with an efficient surface area-to-adsorption capacity ratio of 81.80 m^2/g, yielding 10.54 mg/g in chromium adsorption. While specialized materials like walnut shell biochar may achieve higher q_{max} values (45.45 mg/g) [27], likely due to higher surface areas.

Adsorption Isotherm

The Langmuir model supports the concept of monolayer adsorption, assuming uniform adsorption energies across all sites without interactions among adsorbed ions. It is commonly used to interpret adsorption data, with the RHB demonstrating a strong linear correlation with the Langmuir isotherm as evidenced by a correlation coefficient (R^2) of 0.95, indicating a robust positive linear relationship. The high R^2 and low residual error suggest that the Langmuir isotherm accurately represents experimental data, reflecting monolayer adsorption behavior typical of the Langmuir model. The calculated q_{max} values offer insights into the adsorbent's capacity and affinity for the adsorbate [Figure 5(A)]. The Freundlich adsorption isotherm, depicted in logarithmic form, assesses how well the adsorption data align with this model. The Freundlich model accounts for 96.9% of the variability in $\log_{qe}\backslash\log_{q,}$ signifying an excellent fit (R^2 = 0.96). The slope (1/n) of 1.5397 suggests cooperative adsorption, where adsorption increases with higher adsorbate concentrations, as $1/n > 1$[Fig. 5(B)]. Both the Langmuir and the Freundlich models are well-suited for chromium adsorption. The Langmuir isotherm model determined the maximum monolayer adsorption capacity (q_{max}) for RHB to be 10.54 mg/g, indicating a preference for monolayer adsorption. The Freundlich adsorption isotherm showed a K_L value of 4.040, 1/n value of 1.133, and R^2 value of 0.997 (Table 1).

The dual fit to both Langmuir (R^2 = 0.95) and Freundlich (R^2 = 0.96) isotherm models observed for RHB is noteworthy and suggests a complex, heterogeneous adsorption process that cannot be fully described by a single idealized model [53]. This behaviour is not uncommon in biochar systems but provides important mechanistic insights when examined in detail and compared with other materials.

The Langmuir model assumes monolayer adsorption on a homogeneous surface with uniform binding energies—an idealized scenario rarely achieved in practice. The strong fit (R^2 = 0.95) and q_{max} of 10.54 mg/g indicate that, at low to moderate chromium concentrations, the adsorption behaviour approximates monolayer coverage, likely due to the formation of inner-sphere complexes between chromate ions and surface functional groups (as evidenced by FTIR shifts) [54]. However, the equally strong fit to the Freundlich model (R^2 = 0.96) suggests that surface heterogeneity and multilayer adsorption also play significant roles, particularly at higher concentrations where chromate ions may adsorb onto

already-occupied sites or interact with different functional groups having varying binding affinities.

The Freundlich parameter $1/n$ = 1.133 (> 1) is particularly revealing, as it indicates cooperative adsorption where the binding of one chromate ion enhances the adsorption of subsequent ions. This positive cooperativity can be explained by several mechanisms: (1) initial chromate adsorption may induce conformational changes in the biochar surface that create new binding sites [55], (2) adsorbed chromate ions may form bridges facilitating the binding of additional ions, or (3) electrostatic reorganization following initial adsorption may make neighbouring sites more accessible. This behaviour contrasts with most reported biochar systems, where 1/n values typically range from 0.1 to 0.5, indicating favourable but non-cooperative adsorption [56]. The cooperative nature of chromate binding to RHB may contribute to its high removal efficiency even at elevated concentrations.

The Langmuir constant K_L = 4.040 L/mg indicates a moderately strong affinity between chromate and RHB, consistent with the chemisorption mechanism confirmed by kinetic studies. Comparing this with other biosorbents, the separation factor R_L (calculated as $R_L = 1/(1 + K_L C_O)$, where C_O is the initial concentration) ranges from 0.002 to 0.01 across the tested concentration range (100–500 ppm), all values being much less than 1, confirming highly favourable adsorption conditions. This is superior to many other biochar systems where R_L values closer to 0.1–0.5 are reported, indicating weaker adsorbate-adsorbent interactions [57].

Cross-comparing with literature-reported isotherm data, CSB and CMB, which achieved q_{max} values of 21.24 and 24.28 mg/g, respectively, at pH 6.0, demonstrate higher maximum capacities than RHB (10.54 mg/g) [58]. RHB achieves 91% removal at 0.8 g/L, whereas many higher-capacity materials require 1.5–2.0 g/L for comparable efficiencies. Walnut shell biochar's higher q_{max} of 45.45 mg/g [66] at pH 4–5 demonstrates that surface area and pore structure can be further optimized. However, the 96.5% removal efficiency is only marginally better than RHB's 91%, suggesting diminishing returns on adsorption capacity beyond certain thresholds. The reduced rice straw biochar achieving 95% removal at pH 2 with a q_{max} of 21.43 mg/g illustrates how extreme pH conditions can enhance both capacity and efficiency, though such conditions may be impractical or uneconomical for industrial applications [28].

The isotherm also provides insights into the adsorption mechanism hierarchy. The good Langmuir fit at low concentrations suggests that chemisorption via surface complexation dominates initially, occupying the highest-energy binding sites (primarily hydroxyl and carbonyl groups identified by FTIR). As these sites saturate, the Freundlich model becomes more descriptive, reflecting adsorption onto lower-energy sites and the onset of multilayer adsorption, possibly involving weaker electrostatic interactions and physical adsorption in mesopores. This sequential site occupancy model is supported by the intraparticle diffusion data showing multiple linear regions, each corresponding to different types of adsorption sites being accessed.

Adsorption kinetics and mechanism

To gain a better understanding of the adsorption process, kinetic models were employed. The pseudo-first-order kinetic model as well as the pseudo-second-order kinetic model were employed to reveal the nature of the adsorption process. The results showed that the pseudo-second-order model fitted the experimental data well ($R^2 > 0.98$), indicating that chemisorption might have occurred. The chemisorption process involves the formation of a chemical bond between the functional groups on the biochar surface and the Cr (VI) ions [59].

The intra-particle diffusion model was used to determine the rate-controlling steps in adsorption [53, 54]. This model was used to understand adsorption dynamics in several stages. The stages include external or boundary layer diffusion, in which metal ions move in solution to adsorbent surfaces. Secondly, it includes intra-particle or internal diffusion that refers to ion diffusion inside biochar pores. Finally, there is adsorption that occurs on the adsorbent internal surfaces [54, 60]. Based on this model, intra-particle diffusion kinetics showed linearity that indicates two stages in adsorption. The first linearity is associated with boundary layer diffusion. The other linearity is associated with intra-particle diffusion in biochar. The two straight lines can be considered an indication that adsorption is not governed by intra-particle diffusion alone. Additionally, both external and internal mass transports govern overall adsorption kinetics [61].

The confirmation that chromate adsorption onto RHB follows pseudo-second-order kinetics ($R^2 > 0.98$) provides definitive evidence for a chemisorption-dominated mechanism, distinguishing it from physisorption processes that typically follow pseudo-first-order kinetics [62]. This finding has important mechanistic and practical implications when examined in the context of comparative biochar studies and theoretical adsorption frameworks [63, 64]. The pseudo-second-order model is derived from the assumption that the rate-limiting step involves chemical bonding between adsorbate and adsorbent, such as electron sharing or exchange, covalent bonding, or strong electrostatic interactions. The excellent fit ($R^2 > 0.98$) indicates that the adsorption rate is proportional to the square of the number of unoccupied sites, suggesting that site availability controls the overall process. This contrasts with pseudo-first-order kinetics, where the rate is simply proportional to the number of

unoccupied sites, typical of diffusion-controlled physisorption [62, 65].

The chemisorption interpretation is strongly corroborated by FTIR evidence showing peak shifts and the appearance of new functional groups post-adsorption, indicating chemical bond formation rather than mere physical attachment. The specific involvement of hydroxyl (-OH), amine (-NH_2), and carbonyl (C = O) groups suggests multiple parallel chemisorption pathways, potentially including: (1) ligand exchange where chromate ions displace hydroxyl groups or water molecules from the biochar surface, (2) surface complexation forming inner-sphere complexes with specific functional groups, and (3) reduction-coupled adsorption where Cr (VI) may be partially reduced to Cr (III) by electron-donating groups on the biochar surface, followed by precipitation or further adsorption of Cr (III) [38, 39].

The intraparticle diffusion analysis, revealing two distinct linear stages, provides additional mechanistic depth beyond the pseudo-second-order model. The first linear region corresponds to boundary layer diffusion, where chromate ions move through the stagnant liquid film surrounding biochar particles to reach the external surface (Fig. 6). The second linear region represents intraparticle diffusion, where ions penetrate the pore network. The non-zero intercepts ($C \neq 0$) for both linear regions confirm that intraparticle diffusion alone does not control the overall rate; instead, both external and internal mass transfers contribute to rate limitation. This multi-step mechanism is consistent with the Type IV isotherm and mesoporous structure (3.32 nm pore size) of RHB, which allows for relatively rapid internal diffusion compared to microporous materials [65].

Comparing with other biochar systems, the two-stage diffusion pattern is commonly observed but with varying relative contributions of each stage. Materials with higher surface areas but predominantly microporous structures often show longer secondary (intraparticle diffusion) stages, as smaller pores impede diffusion [66–68]. RHB's mesopore-dominant structure appears to facilitate a better balance, allowing substantial adsorption in both stages without excessive diffusion limitation. This is reflected in the relatively short equilibrium time (120 min) compared to spent coffee ground biochar (180 min) [69] and some activated carbons (> 240 min for similar systems) derived from coconut shell and corn straw biochar [70, 71]. The rate constant from the pseudo-second-order model (k_2), while not explicitly stated in the results, can be estimated from the time to achieve 50% of equilibrium capacity {$t1/2 = 1/(k_2 qe)$}. Based on the kinetic profile showing 83% removal in 30 min and 91% at 120 min, the relatively rapid initial uptake suggests a higher k_2 value than many comparable systems, indicating strong adsorbent-adsorbate affinity and efficient mass transfer characteristics. The identification of chemisorption as the dominant mechanism has important practical implications for industrial applications and biosorbent regeneration [72, 73]. Chemisorption is generally considered irreversible or difficult to reverse under mild conditions, which may complicate biosorbent regeneration but also means that the adsorbed chromium is unlikely to desorb spontaneously, reducing the risk of secondary contamination [59]. For applications where chromium recovery is desired, stronger desorption agents or elevated temperatures would be required compared to physisorption systems, but the stability of binding ensures effective long-term sequestration of chromium.

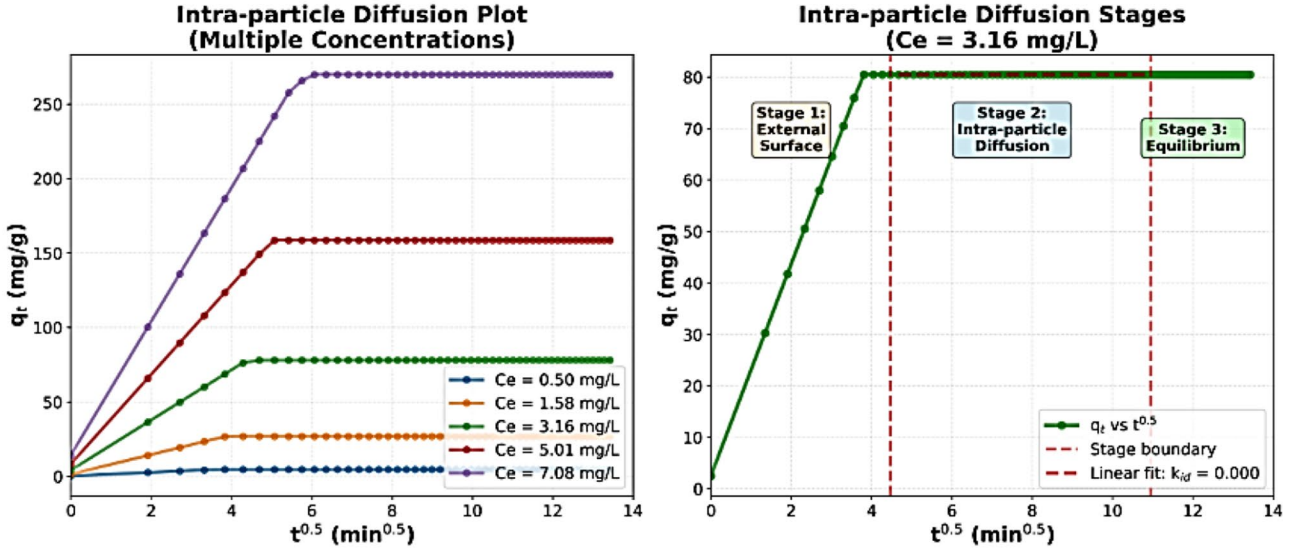

Fig. 6 Intra-particle diffusion plot and intra-particle diffusion stages

Furthermore, the multi-step diffusion mechanism informs reactor design considerations. The significant contribution of external diffusion suggests that agitation intensity and particle size would have notable effects on overall adsorption rates. Smaller particles would reduce diffusion path lengths, while vigorous mixing would reduce boundary layer thickness, both potentially accelerating the process. However, these operational parameters must be balanced against energy costs and particle attrition concerns in continuous treatment systems.

Comparison of RHB with other adsorbents

Table 2 compares RHB with other organic waste adsorbents employed for Cr (VI) removal. RHB is a competent adsorbent in terms of removal efficiency and adsorption capacity. Although there are other adsorbents, like walnut shell biochar [16], Pistachio shell biochar [74, 75], Corn straw biochar, and groundnut hull/husk biochar [29], with higher maximum adsorption capacities, RHB is more advantageous in terms of cost-effectiveness, availability, and conversion of agricultural waste materials. The percentage removal of Chromium by 91% using RHB adsorbent is comparable with other biochar adsorbents, thereby proving the potential, competence, and sustainability of Rice hull biochar in the remediation of Cr(VI).

Utilization of spent biochar and treated wastewater for seed germination studies on *Cicer arietinum*

The study examined the impact of tannery effluent and RHB on plant growth parameters of *Cicer arietinum* (chickpea) (Fig. 7A and B). In Fig. 7, the control showed minimum root and shoot length, number of leaves, and nodules. When biochar residue and effluent were in a 1:1 ratio, minimum growth was observed. When effluent and biochar residue were in ratios of 1:2 and 1:3, there was a slight decrease in growth parameters. However, when biochar residue and effluent were in a ratio of 1:4, a large variation was seen with an increase in root and shoot length, leaves, and node numbers compared to the control. This indicates that when Agri-waste residue was 80% and tannery effluent was 20%, the Agri-waste neutralizes toxic metals and provides nutritional impact, helping in the growth of chickpea seeds. Similarly, Roots and shoots of *Triticum aestivum* L. (wheat) were affected by chromium stress, showing a decrease in root and shoot length [76]. Treatments with biochar made from jujube wood waste biochar (JBC) showed a notable rise in germination percentage when compared to control treatments lacking JBC. Applying jujube wood waste biochar (JBC) to seedlings under severe Cr (VI) increases their root and shoot length because Cr (VI) gets sorbed onto the charged surface of the biochar through electrostatic interaction [76].

Table 2 Comparison of Cr (VI) removal using different biochar adsorbents

Adsorbent	q_{max} (mg/g)	Removal Efficiency (%)	Optimal pH	Reference
Rice Hull Biochar (RHB)	10.54	91	4	This study
Walnut Shell Biochar	45.45	96.5	4–5	[16]
Corn Straw Biochar	21.24	91	6	[27]
Reduced Rice Straw Biochar	21.43	95	2	[28]
Peanut Hull Biochar	12.00	98	3	[75]

The experiment involved harvesting chickpea seedlings for fresh weight and oven-drying for dry weight. The chickpea showed a minimum decrease in fresh mass when the dilution factor of tannery effluent and biochar residue was 50%. The toxic effect of chromium caused an increase and a decrease in fresh and dry weight. The fresh mass increased gradually with an increase in Agri-waste residue, with the maximum increase at a dilution factor of 1:4. In the ratio of 1:2, a reduction in dry weight was recorded, but when the ratio was 1:4, an increase in dry weight was recorded (Figs. 8 and 9). The study found that chickpeas' fresh mass decreased minimally when the tannery effluent and biochar residue dilution factor was 50%, while seedlings' fresh and dry weight increased due to chromium toxicity. Previous studies have shown a decrease in fresh and dry weight of *Helianthus annus* L. and *Gossypium herbaceum* under different chromium toxicity concentrations [77]. Maize straw-derived biochar enhanced seed and overall plant growth, while these parameters were low in control conditions of cadmium toxicity [51].

The seed germination and plant growth studies provide critical validation of RHB's practical applicability for wastewater remediation and agricultural reuse, addressing a gap often overlooked in biosorption research focused solely on removal efficiency. The dose-dependent effects on *Cicer arietinum* growth parameters offer important insights into the dual role of biochar as both a detoxifier and a potential soil amendment. The observation that the 1:1 dilution ratio (50% effluent: 50% biochar residue) resulted in minimum growth, comparable to or worse than the control, indicates residual chromium toxicity despite biochar treatment [78]. This suggests that at high effluent concentrations, biochar's adsorption capacity is overwhelmed, leaving sufficient free chromium to inhibit seed germination and early seedling development. Chromium toxicity in plants manifests through multiple mechanisms, including oxidative stress, disruption of nutrient uptake (particularly iron, manganese, and phosphorus), interference with photosynthesis, presence of other more toxic heavy metals (Pb and Cd) [79], and root membrane damage [80]. The minimal growth at a 1:1 ratio likely reflects these combined toxic effects.

As the dilution factor increased to 1:2 and 1:3, slight improvements in growth parameters were observed,

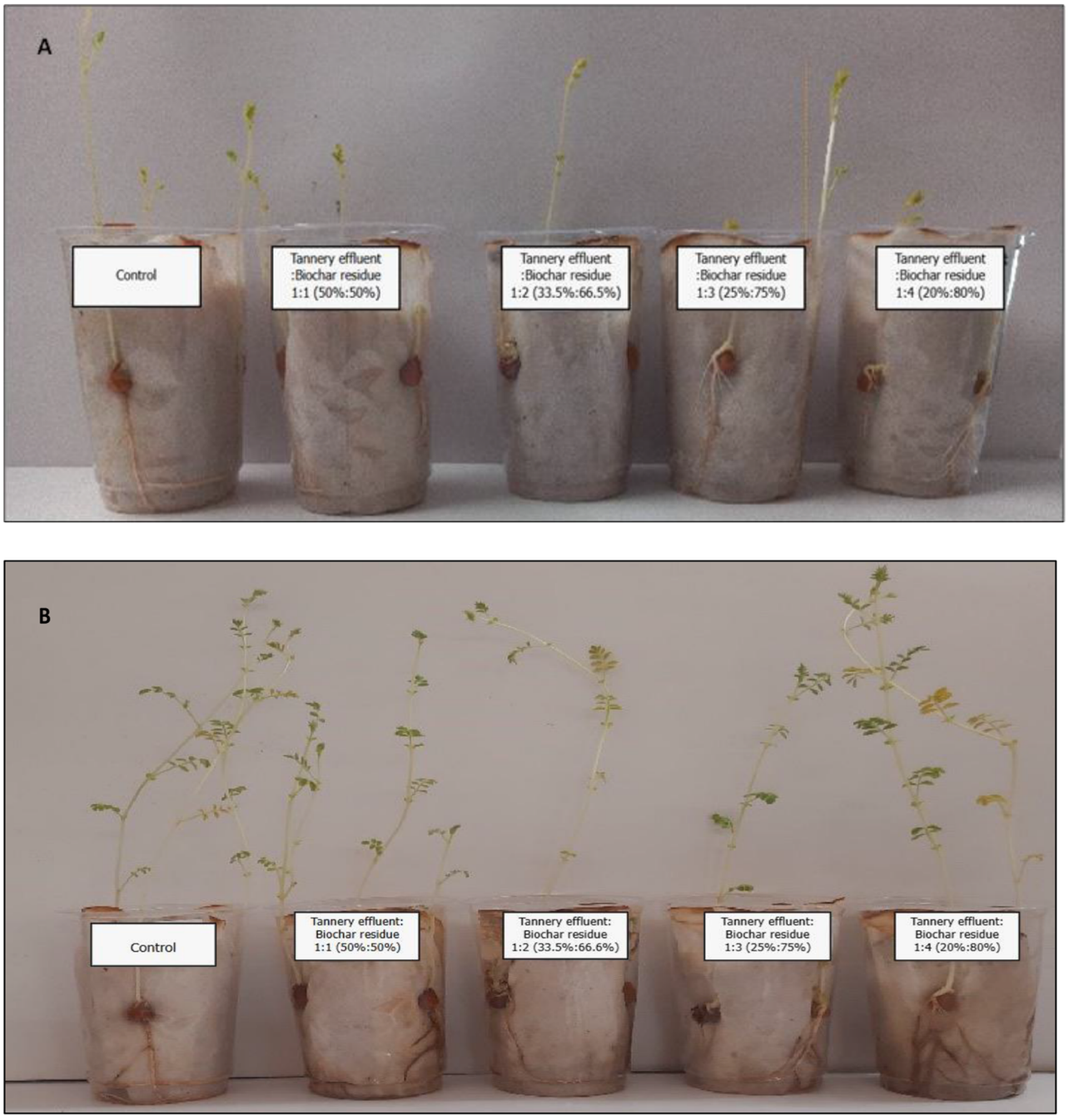

Fig. 7 Growth of Chickpea (*Cicer arietinum*) in various dilution factors of tannery effluent and biochar residue (**A**) On day 7 (**B**) On day 14

indicating progressive reduction in bioavailable chromium to sub-toxic levels. However, the dramatic enhancement observed at the 1:4 ratio (20% effluent: 80% biochar residue), with significantly increased root length, shoot length, leaf number, nodule formation, and biomass compared to controls, suggests a transition from mere toxicity mitigation to active growth promotion [79]. This enhanced growth beyond control levels can be attributed to several synergistic factors: (1) complete chromium immobilization below phytotoxic thresholds, (2) release of essential nutrients (K, Ca, Mg, Fe) from the biochar residue as evidenced by EDS analysis showing these elements in RHB composition, and (3) improved water retention and aeration provided by biochar particles in the growth medium.

Comparison with wheat (*Triticum aestivum L.*) studies using JBC [76] reveals similar protective effects, wherein biochar application under chromium stress increased

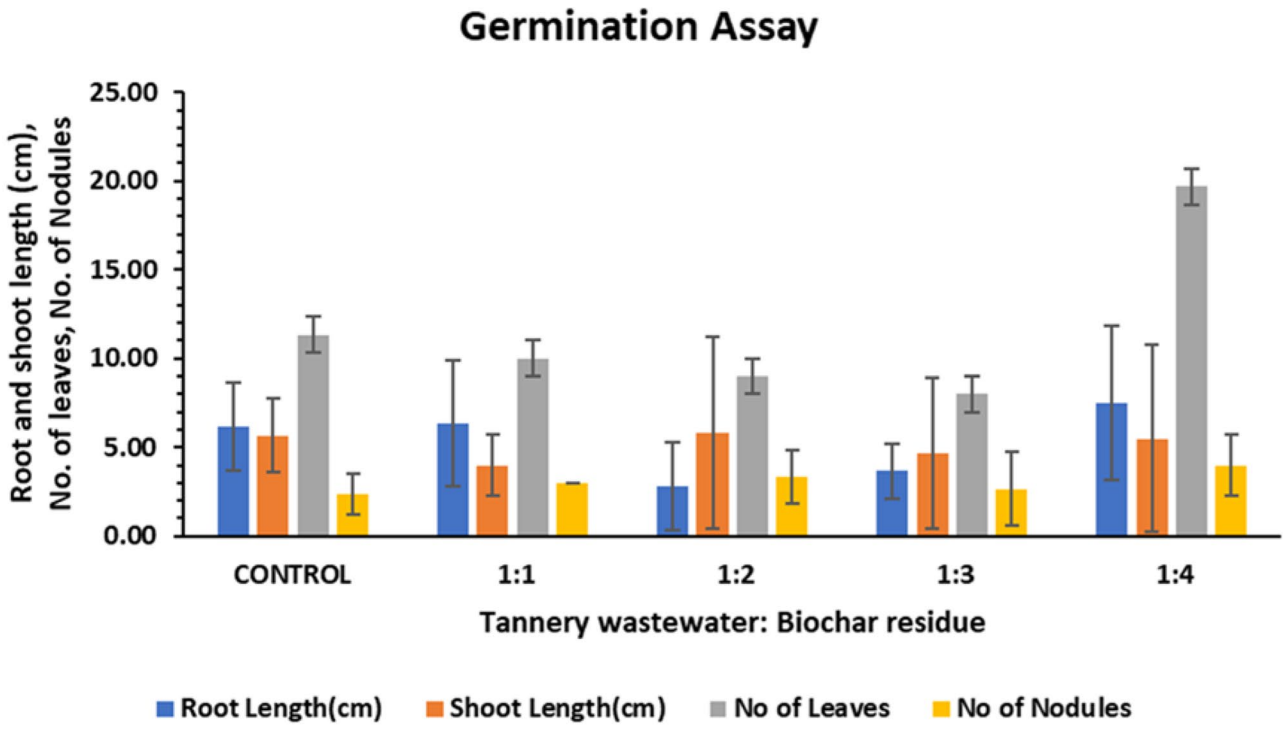

Fig. 8 Root and shoot length (cm), no. of leaves, and nodules of chickpea (*Cicer arietinum*) on day 14

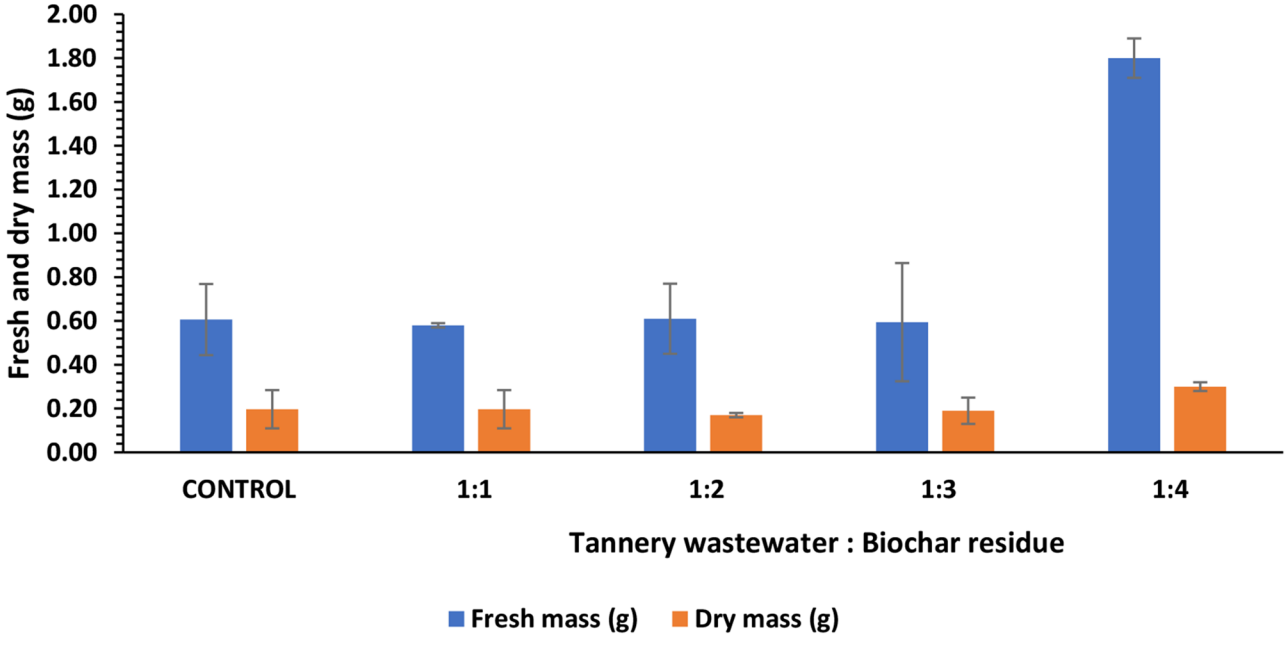

Fig. 9 Fresh and dry mass (g) of chickpea (*Cicer arietinum*) on day 14

germination percentage and root/shoot length through chromium immobilization via electrostatic interaction. However, the chickpea study provides additional nuance by quantifying the dose-response relationship and demonstrating that excessive biochar residue (80%) is not detrimental a concern sometimes raised for biochar soil amendments. The enhanced nodule formation observed at the 1:4 ratio is particularly significant, as legume nodulation is highly sensitive to heavy metal stress. The restoration and enhancement of this symbiotic nitrogen-fixing capability suggest complete alleviation of

chromium toxicity and potentially favourable conditions for Rhizobium activity.

The fresh and dry biomass results provide additional mechanistic insights beyond mere survival and germination. The initial decrease in fresh mass at the 1:1 ratio, followed by progressive increases at higher dilution factors, mirrors the trends in other growth parameters. The maximum increase in both fresh and dry mass at the 1:4 ratio indicates that plants were not only surviving but actively growing and accumulating biomass, contrasting with the stunted growth observed in *Helianthus annus* L. under chromium stress [77]. The increase in dry mass is particularly significant as it represents actual tissue accumulation rather than mere water uptake, confirming genuine growth promotion.

Comparing with maize straw-derived biochar studies, which similarly enhanced seed and overall plant growth compared to control conditions, RHB demonstrates comparable or superior bioremediation and growth-promoting properties [79]. The mechanism likely involves not just chromium immobilization but also improvement of the rhizosphere environment through pH buffering, enhanced cation exchange capacity, and provision of slowly-released nutrients. The agricultural implications of these findings are substantial. They demonstrate that treated tannery effluent, when appropriately diluted with biochar residue, can be safely reused for irrigation without phytotoxic effects, with apparent benefits over control conditions. This addresses a critical challenge in water-scarce regions where wastewater reuse is necessary but heavy metal contamination limits applicability. The 1:4 dilution ratio provides a practical guideline for safe reuse, though field trials under realistic soil conditions would be necessary to validate these findings.

Furthermore, the post-treatment biochar residue itself has value as a soil amendment, providing a dual benefit: chromium immobilization and soil quality improvement. This aligns with circular economy principles, where waste (rice hull) is converted into a remediating agent (biochar) that itself becomes a valuable soil amendment after chromium sequestration [59]. However, long-term studies would be necessary to ensure that chromium remains stably bound to biochar in soil environments and does not remobilize under varying pH, redox, or microbial activity conditions. The absence of any enhanced chromium uptake by plants at the 1:4 ratio (as evidenced by normal to enhanced growth) suggests successful immobilization, though direct measurement of chromium in plant tissues would provide definitive confirmation. Studies on biochar-amended contaminated soils typically show reduced plant chromium uptake due to decreased bioavailable fraction [36, 37], and the current results are consistent with this pattern.

Conclusion

This study concludes that RHB is a potential biosorbent for Cr (VI) removal from tannery wastewater, achieving 91% removal efficiency under optimal conditions (pH 4, 0.8 g/L dosage, 120 min). The studies suggested that RHB has a higher adsorption capacity than other biochar materials because it has a well-developed porous structure, supports pseudo-second-order kinetics, and a two-step adsorption mechanism. Langmuir & the Freundlich isotherm, FTIR, and SEM-EDS analysis confirmed the adsorption mechanism and modification of functional groups. Seed germination trials using treated effluent showed improved growth in *Cicer arietinum* (chickpea), indicating potential agricultural reuse. Future directions include pilot-scale experimentation to verify lab-scale data, research on regeneration methods for biochar use over multiple cycles, long-term experiments to test the safety and efficiency of treated water for reuse, techno-economic analysis, and research on methods to chemically or thermally modify biochar to improve adsorption capacity. The findings address several SDGs (6, 12, 14, and 15) and suggest that rice husk biochar is a scalable, eco-friendly solution for chromium remediation and tannery wastewater recycling.

Abbreviations

BET	Brunauer–Emmett–Teller Analysis
CETP	Common Effluent Treatment Plant
CSB	Corn Straw Biochar
CMB	Cow Manure Biochar
EDS	Energy Dispersive X-Ray Spectroscopy
FESEM	Field Emission Scanning Electron Microscopy
FTIR	Fourier Transform Infra-Red Spectroscopy
RH	Rice Hull
RHB	Rice Hull Biochar
SEM	Scanning Electron Microscopy
SDGs	Sustainable Development Goals

Supplementary Information

The online version contains supplementary material available at https://doi.org/10.1186/s44316-026-00058-1.

Supplementary Material 1

Acknowledgements

This infrastructure facility was provided by DST-FIST (Grant no. SR/FST/LS-I/2019/502) and DST-PURSE (Grant no. SR/PURSE/2021/77), provided to Amity University Rajasthan.

Author contributions

S.Y. Conceptualization, Formal analysis, Resources, Writing – original draft, Writing – review & editing N.K. Formal analysis, Writing – review & editing A.B. Formal analysis, Writing – review & editing, P.K. - Writing – review & editing, Formal analysis G.K.A. (corresponding author) Formal analysis, Resources, Supervision, Writing – review & editing N.J. (Supervisor and corresponding author) Conceptualization, Formal analysis, Resources, Supervision, Writing – original draft, Writing – review & editing.

Funding
This infrastructure facility was provided by DST-FIST (Grant no. SR/FST/LS-I/2019/502) and DST-PURSE (Grant no. SR/PURSE/2021/77), provided to Amity University Rajasthan.

Data availability
No datasets were generated or analysed during the current study.

Declarations

Ethical approval
The article does not contain any studies involving humans or animals.

Use of artificial intelligence (AI)-assisted technology
The authors declare that they have not used artificial intelligence (AI) tools for writing and editing of the manuscript, and no images were manipulated using AI.

Competing interests
The authors declare no competing interests.

Author details
[1]Amity Institute of Microbial Technology, Amity University Rajasthan, Jaipur 303002, India
[2]J-Class Solutions, Inc., Computational Protein Engineer, Danbury, CT 06810, USA
[3]Amity Institute of Biotechnology, Amity University Rajasthan, Jaipur 303002, India

Received: 28 November 2025 / Accepted: 30 March 2026
Published online: 18 May 2026

References

1. Anjum M, Miandad R, Waqas M, Gehany F, Barakat MA. Remediation of wastewater using various nano-materials. Arab J Chem. 2019;12(8):4897–919. https://doi.org/10.1016/j.arabjc.2016.10.004.
2. Ke B, Nguyen H, Bui XN, Bui HB, Choi Y, Zhou J, et al. Predicting the sorption efficiency of heavy metal based on the biochar characteristics, metal sources, and environmental conditions using various novel hybrid machine learning models. Chemosphere. 2021;276:130204. https://doi.org/10.1016/j.chemosphere.2021.130204.
3. Bai XT, Wang J, Dong H, Chen JM, Ge Y. Relative importance of soil properties and heavy metals/metalloids to modulate microbial community and activity at a smelting site. J Soils Sediments. 2021;21:1–12. https://doi.org/10.1007/s11368-020-02743-8.
4. Wang W, Wei P, Wang C, Liang P, Tao F, Yang S, et al. Honeycomb-structured biochar from waste pomelo peel for synergistic adsorptive and photocatalytic removal of Cr (VI). Carbon Res. 2025;4(1):10. https://doi.org/10.1007/s44246-024-00174-5.
5. Mortada WI, El-Naggar A, Mosa A, Palansooriya KN, Yousaf B, Tang R, et al. Biogeochemical behaviour and toxicology of chromium in the soil-water-human nexus: A review. Chemosphere. 2023;331:138804. https://doi.org/10.1016/j.chemosphere.2023.138804.
6. Hegazi HA. Removal of heavy metals from wastewater using agricultural and industrial wastes as adsorbents. HBRC J. 2013;9(3):276–82. https://doi.org/10.1016/j.hbrcj.2013.08.004.
7. Dong FX, Yan L, Zhou XH, Huang ST, Liang JY, Zhang WX, Guo ZW, Guo PR, Qian W, Kong LJ, Chu W, Diao ZH. Simultaneous adsorption of Cr(VI) and phenol by biochar-based iron oxide composites in water: Performance, kinetics and mechanism. J Hazard Mater. 2021;416:125930. https://doi.org/10.1016/j.jhazmat.2021.125930.
8. Verma A, Sharma G, Kumar A, Dhiman P, Stadler FJ. Recent advancements in biochar and its composite for the remediation of hazardous pollutants. Curr Anal Chem. 2025;21(1):15–56. https://doi.org/10.2174/0115734110286724240318051113.
9. Bayuo J, Rwiza MJ, Mtei KM, Choi JW. Adsorptive removal of heavy metals from wastewater using low-cost adsorbents derived from agro-based materials. In: Kumar N, editor. Heavy Metal Remediation. Earth and Environmental Sciences Library. Cham: Springer; 2024. https://doi.org/10.1007/978-3-031-53688-5_11.
10. Parihar DS, Narang MK, Dogra B, Prakash A, Mahadik A. Rice residue burning in northern India: an assessment of environmental concerns and potential solutions–a review. Environ Res Commun. 2023;5(6):062001. https://doi.org/10.1088/2515-7620/acb6d4.
11. Saurabh K, Roy HS, Shubha K, Sundaram PK, Prakash V, Koley TK, et al. Transforming rice straw into eco-friendly growing medium for microgreens: a solution for agricultural waste management. Front Sustain Food Syst. 2025;9:1556396. https://doi.org/10.3389/fsufs.2025.1556396.
12. Joseph M, Moonsammy S, Davis H, Warner D, Adams A, Oyedotun TDT. Modelling climate variabilities and global rice production: a panel regression and time series analysis. Heliyon. 2023;9(4). https://doi.org/10.1016/j.heliyon.2023.e15480.
13. Basri MSM, Mustapha F, Mazlan N, Ishak MR. Optimization of rice husk ash-based geopolymers coating composite for enhancement in flexural properties and microstructure using response surface methodology. Coatings. 2020;10(2):165. https://doi.org/10.3390/coatings10020165.
14. Bayuo J, Rwiza MJ, Choi JW, Njau KN, Mtei KM. Recent and sustainable advances in phytoremediation of heavy metals from wastewater using aquatic plant species: Green approach. J Environ Manage. 2024;370:122523. https://doi.org/10.1016/j.jenvman.2024.122523.
15. Bayuo J, Abukari MA, Pelig-Ba KB. Desorption of chromium (VI) and lead (II) ions and regeneration of the exhausted adsorbent. Appl Water Sci. 2020;10(7):171. https://doi.org/10.1007/s13201-020-01250-y.
16. Kokab T, Ashraf HS, Shakoor MB, Jilani A, Ahmad SR, Majid M, et al. Effective removal of Cr (VI) from wastewater using biochar derived from walnut shell. Int J Environ Res Public Health. 2021;18(18):9670. https://doi.org/10.3390/ijerph18189670.
17. Banerjee S, Misra A, Chaudhury S, Dam B. A Bacillus strain TCL isolated from Jharia coalmine with remarkable stress responses, chromium reduction capability and bioremediation potential. J Hazard Mater. 2019;367:215–23. https://doi.org/10.1016/j.jhazmat.2018.12.038.
18. Moureen A, Waqas M, Khan N, Jabeen F, Magazzino C, Jamila N, Beyazli D. Untapped potential of food waste derived biochar for the removal of heavy metals from wastewater. Chemosphere. 2024;356:141932. https://doi.org/10.1016/j.chemosphere.2024.141932.
19. Burachevskaya M, Minkina T, Bauer T, Lobzenko I, Fedorenko A, Mazarji M, et al. Fabrication of biochar derived from different types of feedstocks as an efficient adsorbent for soil heavy metal removal. Sci Rep. 2023;13(1):2020. https://doi.org/10.1038/s41598-023-27638-9.
20. Abdallah MM, Ahmad MN, Walker G, Leahy JJ, Kwapinski W. Batch and continuous systems for Zn, Cu, and Pb metal ions adsorption on spent mushroom compost biochar. Ind Eng Chem Res. 2019;58(17):7296–307. https://doi.org/10.1021/acs.iecr.9b00749.
21. Jin Y, Zhang M, Jin Z, Wang G, Li R, Zhang X, et al. Characterization of biochars derived from various spent mushroom substrates and evaluation of their adsorption performance of Cu (II) ions from aqueous solution. Environ Res. 2021;196:110323. https://doi.org/10.1016/j.envres.2020.110323.
22. Dias M, Pinto J, Henriques B, Figueira P, Fabre E, Tavares D, et al. Nutshells as efficient biosorbents to remove cadmium, lead, and mercury from contaminated solutions. Int J Environ Res Public Health. 2021;18(4):1580. https://doi.org/10.3390/ijerph18041580.
23. Banerjee S, Kamila B, Barman S, Joshi SR, Mandal T, Halder G. Interlining Cr (VI) remediation mechanism by a novel bacterium Pseudomonas brenneri isolated from coalmine wastewater. J Environ Manage. 2019;233:271–82. https://doi.org/10.1016/j.jenvman.2018.12.048.
24. Din SU, Al-Ahmary KM, Al-Mhyawi SR, et al. Sustainable removal of Cd(II) and Cr(VI) from aqueous solution via agro-waste derived biochar. Sci Rep. 2026. https://doi.org/10.1038/s41598-026-40608-1.
25. Kılıç M, Kırbıyık Ç, Çepelioğullar Ö, Pütün AE. Adsorption of heavy metal ions from aqueous solutions by bio-char, a by-product of pyrolysis. Appl Surf Sci. 2013;283:856–62. https://doi.org/10.1016/j.apsusc.2013.07.033.
26. Murtaza G, Usman M, Ahmed Z, Rizwan M, Iqbal R. Non-wood-based biochars as promising and eco-friendly adsorbents for chromium hexavalent Cr (VI) removal from aquatic systems: state-of-the-art, limitations, and potential future directions. Environ Pollut Bioavailab. 2024;36(1):2387680. https://doi.org/10.1080/26395940.2024.2387680.
27. Xu Q, Xiong C, Fan J, Zhang F, Wang J, Xu Q, et al. Assessing the efficiency and mechanism of copper adsorption onto biochars derived from corn straw and cow manure. Water Air Soil Pollut. 2023;234(6):390. https://doi.org/10.1007/s11270-023-06385-7.

28. Dahiya A, Bhardwaj A, Rani A, Arora M, Babu JN. Reduced and oxidized rice straw biochar for hexavalent chromium adsorption: revisiting the mechanism of adsorption. Heliyon. 2023;9(11). https://doi.org/10.1016/j.heliyon.2023.e21735.
29. Qiu B, Tao X, Wang H, Li W, Ding X, Chu H. Biochar as a low-cost adsorbent for aqueous heavy metal removal: A review. J Anal Appl Pyrol. 2021;155:105081. https://doi.org/10.1016/j.jaap.2021.105081.
30. Zhao D, Zhang S, Deng H, Hu L, Li A, Eco-Friendly, Adsorbent. Insights Into the Performance and Adsorption Mechanisms of Banana Fruit Shaft Biochar for the Removal of Mn (II), Cd (II), Pb (II), and Cu (II). Appl Organomet Chem. 2025;39(3):e70036. https://doi.org/10.1002/aoc.70036.
31. Idowu AA, Temilade FA, Peter A, Vahidhabanu S, Babu BR. Agro waste material as ecofriendly adsorbent for the removal of Zn (II): isotherm, kinetic, thermodynamic and optimization studies. Desal Water Treat. 2019;155:250–258. https://doi.org/10.5004/dwt.2019.23977.
32. Puari AT, Azora A, Octaviani RA, et al. Sustainable heavy metal removal using coffee husk-derived biochar: Response surface optimization and adsorption mechanisms. J Ecol Eng. 2026;27(3):435–50. https://doi.org/10.12911/22998993/211694.
33. Kumar S, Brar RS, Babu JN, Dahiya A, Saha S, Kumar A. Synergistic effect of pistachio shell powder and nano-zerovalent copper for chromium remediation from aqueous solution. Environ Sci Pollut Res. 2021;28:63422–36. https://doi.org/10.1007/s11356-021-15285-4.
34. Kumar P, Singhania RR, Sumathi Y, et al. Investigating innovative techniques for biochar modification to enhance the removal of heavy metals from aqueous environments: a comprehensive review. Clean Techn Environ Policy. 2025;27:3271–93. https://doi.org/10.1007/s10098-024-02962-4.
35. Al-Qahtani KM. Water purification using different waste fruit cortexes for the removal of heavy metals. J Taibah Univ Sci. 2016;10(5):700–8. https://doi.org/10.1016/j.jtusci.2015.09.001.
36. Chung N, Thuy DT, Trang LH et al. Evaluating coffee husk biochar as a sustainable and novel adsorbent for lead and copper in wastewater. Biomass Conv Bioref 2025; 15: 18437–53. https://doi.org/10.1007/s13399-025-06674-7.
37. Jain M, Garg VK, Kadirvelu K. Chromium removal from aqueous system and industrial wastewater by agricultural wastes. Bioremediat J. 2013;17(1):30–9. https://doi.org/10.1080/10889868.2012.731450.
38. Shakya A, Vithanage M, Agarwal T. Influence of pyrolysis temperature on biochar properties and Cr (VI) adsorption from water with groundnut shell biochars: Mechanistic approach. Enviro Res. 2022;215:114243. https://doi.org/10.1016/j.envres.2022.114243.
39. Sanka PM, Rwiza MJ, Mtei KM. Removal of selected heavy metal ions from industrial wastewater using rice and corn husk biochar. Water Air Soil Pollut. 2020;231:1–13. https://doi.org/10.1007/s11270-020-04624-9.
40. Zhang Z, Zhou C, Yang J, Yan B, Liu J, Wang S, Li Q, Zhou M. Preparation and Characterization of Apricot Kernel Shell Biochar and Its Adsorption Mechanism for Atrazine. Sustainability. 2022;14(7):4082. https://doi.org/10.3390/su14074082.
41. Madzin Z, Zahidi I, Talei A, Raghunandan ME, Hermawan AA, Karam DS. Optimising spent mushroom compost biochar for heavy metal removal: Mechanisms and kinetics in mine water treatment. J Water Process Eng. 2025;69:106829. https://doi.org/10.1016/j.jwpe.2024.106829.
42. Hassan MU, Su Q. A solution to chromium toxicity? Unlocking the multifaceted role of biochar. Plants. 2026;15(2):234. https://doi.org/10.3390/plants15020234.
43. Chen F, Guo S, Wang Y, Ma L, Li B, Song Z, Zhang W. Concurrent adsorption and reduction of chromium (VI) to chromium (III) using nitrogen-doped porous carbon adsorbent derived from loofah sponge. Front Environ Sci Eng. 2022;16(5): 57. https://doi.org/10.1007/s11783-021-1491-6.
44. Rahman MM, Adil M, Yusof AM, Kamaruzzaman YB, Ansary RH. Removal of heavy metal ions with acid activated carbons derived from oil palm and coconut shells. Materials. 2022;7(5):3634–50. https://doi.org/10.3390/ma7053634.
45. Chen Y, Liu J, Zeng Q, Liang Z, Ye X, Lv Y, Liu M. Preparation of Eucommia ulmoides lignin-based high-performance biochar containing sulfonic group: Synergistic pyrolysis mechanism and tetracycline hydrochloride adsorption. Bioresour Technol. 2021;329:124856. https://doi.org/10.1016/j.biortech.2021.124856.
46. Wang X, Zhao Y, Deng J, Zhou Y, Yuan S. Study on the influence mechanism of mineral components in biochar on the adsorption of Cr (VI). Fuel. 2023;340:127631. https://doi.org/10.1016/j.fuel.2023.127631.
47. Jiang J, Wang H, Ren J, Deng L, Che D. Effect of inherent alkali and alkaline earth metals in biochar on adsorption of Pb2 + in aqueous solution: different roles of Na/Mg/K/Ca. Sep Purif Technol. 2025;2 354:128766. https://doi.org/10.1016/j.seppur.2024.128766.
48. Choppala G, Bolan N, Kunhikrishnan A, Skinner W, Seshadri B. Concomitant reduction and immobilization of chromium in relation to its bioavailability in soils. Environ Sci Pollut Res. 2015;22:8969–78. https://doi.org/10.1007/s11356-013-1653-6.
49. Tie J, Li W, Liu H, Huang K, Mi X, We M, Hou L. Efficient adsorption and reduction of Cr (VI) by a novel polyaniline modified magnetic iron-based waterworks sludge from aqueous solution. Chem Eng J. 2023;451:137673. https://doi.org/10.1016/j.cej.2022.137673.
50. Shahid M, Shamshad S, Rafiq M, Khalid S, Bibi I, Niazi NK, et al. Chromium speciation, bioavailability, uptake, toxicity and detoxification in soil-plant system: A review. Chemosphere. 2017;178:513–33. https://doi.org/10.1016/j.chemosphere.2017.03.074.
51. Mu L, Zhou H, Yang K, Wang J, Sun S, Lu Z, Wang L, Zhang N, Bao L. Effect of Biochar-Based Organic Fertilizer on the Growth of Maize in Cadmium-Contaminated Soil. Agriculture. 2025;15(5):447. https://doi.org/10.3390/agriculture15050447.
52. Kayranli B. Adsorption efficiency of groundnut husk biochar in reduction of rhodamine B, recycle, and reutilization. Biomass Convers Biorefinery. 2025;15(18):25501–13. https://doi.org/10.1007/s13399-025-06781-5.
53. Kayranli B. Adsorption of textile dyes onto iron based waterworks sludge from aqueous solution; isotherm, kinetic and thermodynamic study. Chem Eng J. 2011;173(3):782–91. https://doi.org/10.1016/j.cej.2011.08.051.
54. Kayranli B. Cadmium removal mechanisms from aqueous solution by using recycled lignocelluloses. Alex Eng J. 2022;61(1):443–57. https://doi.org/10.1016/j.aej.2021.06.036.
55. Afzaal M, Hameed S, Abbasi NA, Liaqat I, Rasheed R, Khan AA, Manan HA. Removal of Cr (III) from wastewater by using raw and chemically modified sawdust and corn husk. Water Pract Technol. 2022;17(9):1937–58. https://doi.org/10.2166/wpt.2022.093.
56. Bachmann SAL, Dávila IVJ, Calvete T, Féris LA. Adsorption of Cr (VI) on lignocellulosic wastes adsorbents: an overview and further perspective. Int J Environ Sci Technol. 2022;19(12):12727–48. https://doi.org/10.1007/s13762-022-03928-z.
57. Bayuo J, Abukari MA, Pelig-Ba KB. Equilibrium isotherm studies for the sorption of hexavalent chromium (VI) onto groundnut shell. IOSR J Appl Chem. 2019;11(12):40–6. https://europub.co.uk/articles/-A-431713.
58. Bayuo J, Rwiza MJ, Mtei KM. Applicability of bio-adsorbents synthesized from maize/corn plant residues for heavy metals removal from aquatic environments: an insight review. EQA. 2023;56(1):15–35. https://doi.org/10.6092/issn.2281-4485/16951.
59. Guo X, Liu A, Lu J, Niu X, Jiang M, Ma Y, Liu X, Li M. Adsorption Mechanism of Hexavalent Chromium on Biochar: Kinetic, Thermodynamic, and Characterization Studies. ACS Omega. 2020;5(42):27323–31. https://doi.org/10.1021/acsomega.0c03652.
60. Akiode OK, Adetoro A, Anene AI, Afolabi SO, Alli YA. Methodical study of chromium (VI) ion adsorption from aqueous solution using low-cost agro-waste material: isotherm, kinetic, and thermodynamic studies. Environ Sci Pollut Res. 2023;30(16):48036–47. https://doi.org/10.1007/s11356-023-25706-1.
61. Barkat M, Nibou D, Chegrouche S, Mellah A. Kinetics and thermodynamics studies of chromium (VI) ions adsorption onto activated carbon from aqueous solutions. Chem Eng Process: Process Intensif. 2009;48(1):38–47. https://doi.org/10.1016/j.cep.2007.10.004.
62. Simonin JP. On the comparison of pseudo-first order and pseudo-second order rate laws in the modeling of adsorption kinetics. Chem Eng J. 2016;300:254–63. https://doi.org/10.1016/j.cej.2016.04.079.
63. Hassan M, Liu Y, Naidu R, Parikh SJ, Du J, Qi F, Willett IR. Influences of feedstock sources and pyrolysis temperature on the properties of biochar and functionality as adsorbents: a meta-analysis. Sci Total Environ. 2023;858:159946. https://doi.org/10.1016/j.scitotenv.2020.140714.
64. Hu Q, Zhang Z. Application of Dubinin–Radushkevich isotherm model at the solid/solution interface: a theoretical analysis. J Mol Liq. 2019;277:646–8. https://doi.org/10.1016/j.molliq.2019.01.005.
65. Wan J, Liu F, Wang G, Liang W, Peng C, Zhan W, Yang J. Exploring different mechanisms of biochars in removing hexavalent chromium: sorption, reduction and electron shuttle. Bioresour Technol. 2021;337:125382. https://doi.org/10.1016/j.biortech.2021.125382.
66. Dai J, Zhang H, Chen N, Wang Y, Wang J, Yang Z, Fang G. Nitrogen configurations driving efficient elimination of Cr (VI) by nitrogen-doped biochar/zerovalent iron composites. Chem Eng J. 2025;515:163655. https://doi.org/10.1016/j.cej.2025.163655.

67. Liu X, Li Z, Zhang Y, Feng R, Mahmood IB. Characterization of corncob-derived biochar and pyrolysis kinetics in comparison with corn stalk and sawdust. Bioresour Technol. 2023;369:128545. https://doi.org/10.1016/j.biortech.2014.07.077.
68. Shakoor MB, Khalil U, Ali S, Sharif F, Ahmad SR, Rizwan M, Sarker PK. Microwave-assisted magnetic biochar for removal of hexavalent chromium from aqueous solution. Environ Pollut Bioavailab. 2024;36(1):2368590. https://doi.org/10.1080/26395940.2024.2368590.
69. Nguyen VT, Vo TDH, Nguyen TB, Dat ND, Huu BT, Nguyen XC, Tran T, Le TST, Vigneswaran S, Rinklebe J, Ngo HH. Adsorption of norfloxacin from aqueous solution on biochar derived from spent coffee ground: Master variables and response surface method optimized adsorption process. Chemosphere. 2023;288:132577. https://doi.org/10.1016/j.chemosphere.2021.132577.
70. Zahra S, Mahmood Z, Deeba F, Sheikh A, Bukhari H, Mehtab H. Modification of coconut shell charcoal for metal removal from aqueous solutions. Eur J Chem. 2022;13(3):259–66.
71. Tan G, Sun W, Xu Y, Wang H, Xu N. Sorption of mercury (II) and atrazine by biochar, modified biochars and biochar based activated carbon in aqueous solution. Bioresour Technol. 2024;392:129208. https://doi.org/10.1016/j.biortech.2016.03.147.
72. Qiu B, Tao X, Wang H, Li W, Ding X, Chu H. Biochar as a low-cost adsorbent for aqueous heavy metal removal: a review. J Anal Appl Pyrol. 2022;163:105466. https://doi.org/10.1016/j.jaap.2021.105081.
73. Mohadi R, Palapa NR, Taher T, Siregar PMSBN, Juleanti N, Wijaya A, Lesbani A. Removal of Cr (VI) from aqueous solution by biochar derived from rice husk. Commun Sci Technol. 2021;6(1):11–7. https://doi.org/10.21924/cst.6.1.2021.293.
74. Yadav S, Kundu N, Bhattacharya A, Aseri G, Dutta K, Jain N. Valorization and optimization of Pistachio Shell Biochar for Sustainable Reduction of Hexavalent Chromium [Cr(VI)]. J Exp Biol Agri Sci. 2025;13(2):229–38. https://doi.org/10.18006/2025.13(2).229.238.
75. Tabana L, Kupa A, Tichapondwa S. Adsorption of hexavalent chromium from wastewater using magnetic biochar derived from peanut hulls. Phys Chem Earth Parts A/B/C. 2025;137:103815. https://doi.org/10.1016/j.pce.2024.103815.
76. Rafique MI, Ahmad M, Al-Wabel MI, Ahmad J, Al-Farraj A. Mitigating the toxic effects of chromium on wheat (Triticum aestivum L.) seed germination and seedling growth by using biochar and polymer-modified biochar in contaminated soil. Sustainability. 2022;14(23):16093. https://doi.org/10.3390/su142316093.
77. Monisha S, Sangeetha SP. Analysis of Plants, Helianthus annuus (Sunflower) and Gossypium herbaceum (Cotton), for the Control of Heavy Metals Chromium and Arsenic Using Phytoremediation Techniques. Nat Environ Pollut Technol. 2025;24(2):B4237. https://doi.org/10.46488/NEPT.2025.v24i02.B4237.
78. Ren B, Han X, Jin Y, Zhang Y, Song X, Zhao L, Liu R. Synergistic enhancement of agricultural waste biochar in Cr (III)/methylene blue co-pollutant systems: Structure regulation and co-adsorption mechanistic insights. J Environ Chem Eng. 2025;13(5):118989. https://doi.org/10.1016/j.jece.2025.118989.
79. Wu J, Wang T, Wang J, Zhang Y, Pan WPA. novel modified method for the efficient removal of Pb and Cd from wastewater by biochar: Enhanced the ion exchange and precipitation capacity. Sci Total Environ. 2022;754:142150. https://doi.org/10.1016/j.scitotenv.2020.142150.
80. Yadav S, Saleem H, Ibrar I, Naji O, Hawari AH, Alanezi AA, Zaidi SJ, Altaee A, Zhou J. Recent developments in forward osmosis membranes using carbon-based nanomaterials. Desalination. 2023;552:116416. https://doi.org/10.1016/j.desal.2020.114375.

Publisher's note

Springer Nature remains neutral with regard to jurisdictional claims in published maps and institutional affiliations.